



City Research Online

City, University of London Institutional Repository

Citation: Faghih, F. & Ayoub, A. (2019). Structural performance of steel-concrete sandwich beams with carbon nanofiber reinforcement. *Engineering Structures*, 187, pp. 177-198. doi: 10.1016/j.engstruct.2019.02.051

This is the accepted version of the paper.

This version of the publication may differ from the final published version.

Permanent repository link: <https://openaccess.city.ac.uk/id/eprint/21823/>

Link to published version: <https://doi.org/10.1016/j.engstruct.2019.02.051>

Copyright: City Research Online aims to make research outputs of City, University of London available to a wider audience. Copyright and Moral Rights remain with the author(s) and/or copyright holders. URLs from City Research Online may be freely distributed and linked to.

Reuse: Copies of full items can be used for personal research or study, educational, or not-for-profit purposes without prior permission or charge. Provided that the authors, title and full bibliographic details are credited, a hyperlink and/or URL is given for the original metadata page and the content is not changed in any way.

City Research Online:

<http://openaccess.city.ac.uk/>

publications@city.ac.uk

Structural Performance of Steel-Concrete Sandwich Beams with Carbon Nanofiber Reinforcement

Faezeh Faghih¹ and Ashraf S. Ayoub²

¹ Doctoral Candidate, Dept. of Civil Engineering, City, University of London, London, UK

² Professor, Dept. of Civil Engineering, City, University of London, London, UK

Abstract

Cementitious materials such as concrete are typically characterised as quasi-brittle with low tensile strength and low strain capacity, which hence affect the long-term durability of the structure. One of the most important issues in designing and maintaining massive concrete structures like offshore and nuclear power plants is concrete cracking, which is due to the low tensile strength of concrete. This can destroy the structural aesthetic and lead to deterioration of the structure.

The addition of fibers to concrete has been proven to be a good mean to control its crack behaviour and maintain its ductility in tension. Further, since the discovery of carbon nanotubes/fibers (CNT/CNF), they have been also considered as efficient fibers for construction materials such as concrete.

This study presents the structural performance of steel-concrete (SC) elements with a fiber reinforced concrete (FRC) core using both single and hybrid fibers (i.e. consisting of two types of fibers). For this study carbon nanofibers, and steel fibers which are conventionally used in practice, are used for the FRC. Static tests were conducted on eight SC beams with different concrete types. The paper reports on the experimental results obtained from four-point flexural loading of the SC beams. The study shows considerable improvement for both the strength and ductility of the tested specimens. The research laid the groundwork for additional in-depth studies on using carbon nanofiber reinforced concrete within structural members.

Keywords: Steel-concrete sandwich beam (SC); Carbon nanofiber (CNF); Carbon nanofiber reinforced concrete (CNFRC); steel fiber (SF); cracking; shear

1. Introduction

Steel plate composite construction is a sandwich system in which two steel plates encase the concrete in the middle. The composite action is provided by shear studs. The SC system was originally devised for use in submerged tube tunnels over 25 years ago by a team of local consultants in Cardiff, UK. The two face plates act as permanent formwork during construction providing impermeable skins, which are highly suited for marine and offshore applications [1].

One of many advantages of SC systems over the conventional RC construction is the elimination of the time and workmanship required for constructing the formwork, placing rebars and removing the formworks as the steel plates act as formwork themselves. Further, sections can be modularised and prefabricated off-site. Using SC systems reduces the cost of reinforcement with savings resulting from less workmanship required for the construction process. Takeuchi et al. [2] conducted a feasibility study and they found that in SC structural systems a decrease in the amount of steel by about 20% is possible and additional formworks become unnecessary for this type of construction compared to RC structures. The construction period was also estimated to be 2-5 months shorter than RC structures.

According to Oduyemi and Wright [3] and Liew et al. [1], this form of construction combines the advantages of both steel and reinforced concrete, and is thought to give increased impact and blast resistance in installations subject to such loads. SC system application is diverse including nuclear containments, liquid and gas retaining structures, submerged tunnel linings, building cores, the basement of multi-storey buildings, bridge deck, floating breakwater, and offshore structures, which all are required to be blast resistant [1, 4]. In particular, the Westinghouse AP 1000 SC wall modules are being used in nuclear power plant industry as well as Bechtel's proprietary design for SC walls. In nuclear power plant infrastructure, the SC modules have been proposed for use primarily as shear wall structures inside and outside containment. The loads that should be considered acting on these structures are dead load, live load, pressure loads, seismic loads, blast loads, and thermal loads. For research studies covering SC systems, particular emphasis is given to research focusing on properties of out-of-plane flexural strength, shear strength, and bending stiffness. The aim of this research is to enhance the properties of SC structural elements through the use of fiber reinforcement in the concrete core. The paper presents the experimental investigation on out-of-plane flexural performance of SC beams with a hybrid FRC concrete core consisting of conventional steel fibers and carbon nanofibers.

Nanotechnology has been applied to cementitious materials in the last decade, successfully enhancing many properties such as the durability and strength, as well as introducing new capabilities such as self-sensing. Cracks in cement-based materials initiate from the nanoscale where microfibers are not effective. Therefore, the development of fibers at the nanoscale has opened a new field of research within cementitious materials in the past two decades. The idea of a hybrid fiber reinforced concrete,

in which two or several types of fibers, likely in different scales (e.g. nano/micro/macro), are included in the matrix is to take advantage of the benefits from the different fibers and enhance material properties at different structural levels. Considering the cracks initiate at the nano scale, it is aimed in this research to use a combination of nanofibers and conventional steel fibers.

Carbon nanofibers (CNF) are unique as they combine microscopic length (from 200 nm to 100 μm) with a nanoscopic diameter (1–200 nm), with greater strength to weight ratio than steel [5]. CNFs have a lower production cost (about 100 times lower) than other nanofibers such as nanotubes, hence they are suitable for mass production. Additionally, CNFs present numerous exposed edge planes along the surface, and graphene planes are canted from the fiber axis, which in turn create exposed edge planes on the exterior surfaces of the fiber with potential sites for advantageous physical interaction with the matrix.

The nano-reinforced cementitious composite could only benefit from the outstanding properties of the nanofibers when they are properly dispersed within the matrix. The difficulty in dispersing nanofibers in liquid media has been overcome by using methods such as surface modification of fibers using surfactants in combination with sonication. The dispersion and interfacial bond of CNF fibers and cementitious composite at CNF/cement weight ratio of 0.4% were investigated through experiments [6-7]. CNFs were dispersed in a water-surfactant solution and ultrasonically processed for 15 minutes. As the experimental results showed, a polycarboxylate-based superplasticiser (i.e. weaker surfactant also known as water reducing admixture) could properly disperse a relatively high concentration (more than 1.0%) of CNFs in water.

Camacho-Ballesta et al. [8] conducted the dispersion by mixing CNT and distilled water in a high-shear mixer for 10 min and afterward an ultrasound treatment was applied for 5 min. They found a 7.7% improvement in compressive strength of 0.25% CNT reinforced cement paste, while the flexural strength was improved by 19.4% when 0.5% fiber dosage was used. Tyson et al. [9] conducted small-scale flexural tests on CNF reinforced cement paste. It was found that the addition of CNF improved the peak displacement up to 150% (specimen with 0.2 wt% CNF) which is crucial for structural applications in which higher ductility and strain capacity is needed. In addition, the elastic modulus of cement paste was increased from 15 GPa to 24 GPa by addition of 0.2% CNF. In another study, Metaxa et al. [10] investigated the mechanical performance and dispersion of CNF (0.048 wt%) reinforced cement paste. Initially, CNFs were added to a water/surfactant solution then subjected to an intensive sonication. It was concluded that the addition of CNF to cement paste offers a significant property enhancement to the cementitious nanocomposites, mainly increased flexural strength and stiffness, and crack control at the nanoscale. Yazdani and Mohanam [11] studied the compressive strength and flexural strength of cement mortar reinforced with 0.1% and 0.2% of CNF. The mixing technique used was ultrasonication of fibers in the water-surfactant mixture for 15 min. It was

concluded that the best combination for compressive and flexural strength production was CNF composites (0.1%-0.2%) with w/c ratio of 0.35. Gao et al. [12] investigated the mechanical properties of concrete and Self-Consolidating Concrete (SCC) containing 0.16%-2.5% CNF by volume of binder. The cylinder compressive strength of the concrete was increased by 42.7% for 0.16% CNF concentration. The authors believe that using SCC improved CNF dispersal and increased the electrical sensitivity of the concrete. Sivakumar [13] used 0.5%, 1.0%, 1.5%, and 2.0% of CNF by volume of binder within SCC. CNF were mixed with water using a blender, and superplasticiser was then added. The characteristic compressive strength of the concrete increased by 29.4% for 1.0% CNF. Both flexural strength and split tensile strength increased with 0.5% and 1.0% then decreased for higher volume fractions.

Howser et al. [14] tested short shear critical columns built with 1% dosage of CNF reinforced self-consolidating concrete (SCCNFC) under reversed cyclic load. Steel fiber reinforced SCC (SCSFC) and SCC columns with no fibers (SCRC) were also tested for comparison purposes. A definite yielding of longitudinal steel occurred in both the SCRC and SCCNFC columns with visible compression strut, while steel fiber reinforced columns failed with one dominant shear crack. This was attributed to the absence of transverse shear ties. The ultimate normalised capacity, deflection, and ductility of SCCNFC column was respectively 30.7%, 34.9%, and 35.1% higher than the SCRC column. It was concluded that the addition of carbon nanofibers to concrete increased the strength and ductility of the short column.

The effectiveness of silica fume in maintaining a good dispersion was also proposed and studied by researchers [5, 15, 16]. This novel and effective method of using silica fume to immobilise and stabilise the nanofilaments already dispersed in cement paste prevent them from migrating towards each other. Kim et al. [16] studied the SEM images of dispersed CNTs in the cement matrix and it was found that using silica fume strongly affected the mixing process of nanofibers, and they were dispersed individually, hence increasing the compressive strength. The study by Sanchez and Ince [5] on the effect of silica fume on the dispersion enhancement of the CNF in cement composite revealed that silica fume particles due to their small size disrupted the individual CNF fiber-fiber interaction that held them as clumps during the dry mixing. This resulted in an overall greater, though not complete, dispersion of the CNFs throughout the cement paste.

2. Research Significance

The main inspiration for this research was to extend the study on the structural behaviour of SC beams by incorporating the use of nano materials in the matrix to benefit from the advantages of the new smart concrete. Previous research has been carried out on SFRC SC elements, however on a limited

basis. Therefore, the research will focus on the enhancement of SC elements with the use of advanced materials.

3. Experimental Program

The experimental investigations in this paper focus on the out-of-plane flexural behaviour of a typical SC beam in a structure subjected to the postulated loading. In a nuclear structure, SC walls are used in containment buildings, which are subjected to an internal pressure at specific sections. In such structures, the concrete thickness is typically between 600 mm to 1500 mm to provide adequate radiation shielding. In marine or offshore structures, also the SC walls are subjected to lateral loads in the form of lateral pressure. In this research, samples were designated as a beam element subjected to four-point flexural loading. Eight SC beams were designed and tested. Beam specimens were identified as SCB1 through SCB8. The samples were constructed and tested under four-point flexural loading. The SC sandwich beam samples used in this study consisted of two steel plates, which were connected by tie bars to serve as an out of plane shear reinforcement. In this system, the plates are anchored to concrete using headed shear studs, providing composite action between concrete and the steel plates. The use of tie bars connecting the plates also eases specimen handling and construction as the beam itself acts as a mould. A schematic section of a typical SC wall is shown in Figure 1. All beams were intended to have identical dimensions while the type of the concrete core varied for each beam to evaluate the effect of FRC on the structural performance.

All eight samples were divided into three categories (Category1 – Category3) according to their concrete core type. One control sample was constructed with plain concrete for comparison purposes. All concrete types used for the beams are summarised in Figure 2. Each beam was then prepared, tested and the results for each test were recorded. Also, for each SC beam sample, the mechanical properties of the concrete core were obtained by conducting material tests.

To achieve a comprehensive insight into the effect of FRC on structural performance of SC beams in terms of cracking behaviour and failure mode, knowing that the shear mode of failure is the one to be avoided; and with the aim of altering this failure mode by enhancing the material properties, the control beam was initially designed to be shear-critical with plain concrete (with characteristic cylinder compressive strength of 55 MPa). Therefore, the effect of FRC on enhancing the performance of a shear-critical structure could be better observed and analysed. This design was achieved by controlling the vertical shear reinforcement ratio (tie bar diameter; d_{bar} , and tie bar spacing; S) and keeping these parameters within the range that would result in a beam with lower shear capacity than the moment capacity. The design assumptions were:

- Concrete resists no tension,
- Concrete core and steel plates are fully bonded,

- Steel plates do not contribute to the transverse shear capacity.

The final designed beam was fabricated by Arromax Structures Limited. The tie bars ($\varnothing = 6$ mm) and shears studs ($\varnothing = 10$ mm) were welded to two steel faceplates according to the designed dimensions. Specifications of SC beam layout and its components are shown in Figure 3, and geometrical details are presented in Table 1.

To address the aim of this study regarding the effect of FRC on the structural performance of SC wall systems, SC beam elements were prepared to be tested with fiber reinforced concrete (FRC) core. The FRC consisted of single and hybrid fibers, in which a combination of macro and nano-scale fibers was used. The use of hybrid FRC was aimed at further clarifying the effect of fibers of different scales (nano and macro) on the structural performance of the SC beam. For the purpose of this study, steel fibers (SF) and carbon nanofibers (CNF) were used for both singly reinforced concrete and hybrid FRC. Steel fibers have been studied extensively in the past decades and used in the industry, therefore, this type of fiber which is promising to be efficient in improving both, the material properties of concrete and the structural performance of concrete elements, was used as the macro fiber for this experimental investigation.

3.1. Constituent Materials and Mix Proportions

For binder materials, Type I Portland cement, and dry undensified silica fume Grade 940U (Elkem Materials, Inc.) were used with bulk density of 200-350 kg/m³ (Table 2). Silica fume acts physically as a filler and chemically as a highly reactive pozzolan. Sharp sand was used as fine aggregate and gravel with maximum size of 10mm was used as coarse aggregate.

The steel fibers were supplied under the commercial name Dramix 4D by Bekaert Maccaferri. These fibers were originally glued together for mixing purposes to prevent fiber balling during the mixing process. The glue is water sensitive and the fibers will break up into individual fibers and will spread throughout the concrete mix providing a homogenous fiber reinforced concrete. The fibers had the nominal properties tabulated in Table 3.

Heat treated carbon nano fibers (Pyrograf-III, PR-19-XT-LHT) were provided by Applied Sciences Inc. The properties of CNF used in this experimental study are summarised in Table 4. These fibers are heat-treated to temperatures of 1500°C, which carbonizes chemically vapor deposited carbon present on the surface of the fiber to a short-range ordered structure. This heat treatment produces nanofibers which generally provide the highest electrical conductivity in nanocomposites, hence are considered to be better options for smart concrete. The fibers generally become entangled during growth because they are produced in a vapour phase, thus, producing a mesh-like configuration. This raw form is then de-bulked by the manufacturer with a product that is uniform in bulk density

allowing accurate compounding into the final products. The de-bulked form is denoted as XT. The loose bundle of the 'XT' carbon nanofiber requires much less energy to achieve dispersion, thus allowing greater retention of fiber length during processing. The surfactant used for dispersion of CNF in water was a high-range polycarboxylate-based water-reducer admixture (superplasticiser) provided by Elkem under the commercial name ViscoFlow 1000.

Concrete was prepared in a single batch for each beam specimen labelled SCB1 through SCB8. For each batch, 6 cubes and 6 cylinders were also prepared. Uniaxial compression tests were performed on cubes at the age of 14 days and 28 days (i.e. SC beam testing day) to quantify the compressive strength of the concrete core, whereas split tensile test was performed on cylinders at the age of 14 days and 28 days to quantify the tensile strength of the concrete core. The same concrete mix proportions were used for all concrete types, however, due to using different fibers at different dosages, the workability of the mixture was influenced depending on the fiber content (V_f). Therefore, the workability was enhanced after the slump test by adjusting the water demand whenever needed. The mix proportions for each SC beam are shown in Table 5.

3.2. Preparation of CNF and Dispersion in Mixing Water

According to previous research findings, High Range Water Reducer (HRWR) was used to achieve a better dispersion of CNF in aqueous solution. In this study, the HRWR along with ultrasonication was adopted to achieve a good dispersion of the nano fibers in the liquid medium. As Yazdanbakhsh [15] states, 'superplasticiser should not be added to the paste during paste mixing and is required to be added to the aqueous solution to yield the best possible dispersion' of CNFs in water during ultrasonic processing. Therefore, the aqueous solution was made by the following steps:

- a) Water + HRWR; stirred manually
- b) CNF was added; stirred manually for about 2 minutes
- c) Ultrasonication process

A 20-kHz ultrasonic processor (Vibra-Cell, Model VCX 750, Sonics & Materials) was used to disperse the nano fibers using a 139mm long titanium alloy solid probe with 13mm diameter. The processor was set to operate at an amplitude of 50% at 20s time intervals to prevent overheating of the solution. The CNFs were weighed in a glass container then water+HRWR liquid was added and stirred manually. The solution of water+HRWR+CNF was sonicated for about 15 min which was the optimum time needed to achieve well-dispersed CNF/water solution at room temperature.

3.3. Testing Procedure

The instrumentation and test set-up are described next.

3.3.1. Instrumentation

Strain gauges were used for monitoring strains during the test, both inside and on the surface of the beam. Small steel strain gauges FLK-6-11 (6mm long, with a resistance of 120 Ω and a gauge factor of 2.12) provided by Techni Measure were affixed on the tie bars and the bottom plate at different locations as shown in Figure 4. A total of 16 strain gauges were attached to the tie bars located in the shear span (2 gauges on 8 tie bars and a total of 6 gauges were attached to the outer surface of the bottom steel plate).

Each wire connected to a strain gauge was numbered and annotated from G1 to G24 to collect data accordingly. G1-G16 represents gauges on tie bars within the SC beam, G17-G22 represents the strain gauges of the bottom steel plate. The position of steel strain gauges and their numberings are illustrated in Figure 5. This arrangement was consistent for all beams.

The steel plates of the beam were acting partially as formworks and they made the concrete casting and removal easy. A wooden mould was made consisting of a base to cover one face of the beam and additional wood plates were secured at the ends to enclose the sides of the beam. Bracing was installed in the centre to prevent uplift during the cast. Prior to placing the concrete, only the wooden base of the formwork was treated with oil. Concrete was poured in layers and a hand-held electric flexible shaft vibrator was used to achieve a good compaction of concrete. The top surface of the beam was finished and the sample was covered with a plastic cover to avoid water evaporation. The sample was left inside the mould for two days and then removed after making sure that the concrete was set and the de-moulding process would not damage the specimen. The beam was then cured for 28 days with spraying water on the surface of the concrete every 3 days. As stated before, with each beam preparation, 6 cubes and 6 cylinders were also prepared for obtaining the mechanical properties of the concrete.

3.3.2. Test Set-up

After 28 days of curing, the beam was painted in a white colour to better track the formation of cracks during the test, and then it was loaded in the testing frame. A Universal open structure flexural frame with maximum loading capacity of 300kN from CONTROLS Group was used for conducting the four-point bending test on SC beams. The beam span was 1400 mm with a 200 mm overhang. The shear span was 450 mm and the load bearing distance was 500 mm (Figure 6). Strain gauge wires, numbered from G1-G22 were connected to 22 channels of a data logger connected to a PC, logging the strain output automatically at every 1 second. The load was applied in a load control manner with a rate of 80 N/s up to 50kN. Afterwards, the load was applied in a displacement control manner with the rate of 2 μ m/s for higher precision.

4. Results and Discussions

4.1. Concrete Core Material Properties

The results for cubes tested under uniaxial compression and for cylinders under split tensile test at the age of 14 days and 28 days (i.e. SC beam testing day) for each concrete batch are presented in a tabular form in Figures 7 and 8 respectively. The results are the average value of three tested samples. Figure 9 presents the density of each concrete batch.

From Figure 7, the compressive strength of hybrid FRC materials incorporating CNF+SF was less than the PC and CNFRC, which is most likely attributed to the higher water content (i.e. ranging $W/B=0.32-0.39$) used in these mixes for adjusting the workability. Having said that, these materials had the highest split tensile strength due to the fiber bridging effect. The use of hybrid fibers was more effective in enhancing the split tensile strength since the steel fibers could bridge the cracks at the macro scale, at which the nanofibers are ineffective.

Figure 9 shows that with the addition of fibers, the concrete density increased. This effect was the most when 1.5% SF was used in the mix for SCB6. Therefore, the use of high dosage of steel fiber could lead to a higher self-weight of the concrete material while the effect of CNF on the concrete self-weight was less.

The compressive strength of CNFRC with 0.5% (SCB3) and 1% (SCB4) did not show any improvement, which is thought to be due to carbon admixture clusters that might appear after being added to the cement and other concrete constituents.

4.2. SEM Analysis of SC Concrete Core

To gain insight into the microstructure of the concrete, for each SC beam, concrete pieces as samples taken from the cracked sections were inspected by the Scanning Electron Microscopy (SEM) method at Queen Mary University. All samples were inspected as taken from the specimen without any polishing. Below is the discussion on the SEM observations for each sample. A well-dispersed nanofiber is identified by observing individual fibers within the matrix without any agglomeration and dense bundles of the nanofibers. The SEM images of core samples from SCB3 and SCB4 at a fractured surface are illustrated in Figure 10. The figure depicts the insertion of CNFs (arrows) between hydration products, which indicates that the fibers have not been pulled out. A few fibers, however, were pulled out as shown. The figures indicate good fiber-matrix interfacial bond, which could be due to the roughened surface of fibers as a result of sonication as Yazdanbakhsh et al. [6] stated. This also indicates that the bond strength was controllable and can reach a high value to prevent fiber slippage. The energy dissipation takes place at the nanofiber-matrix interface when the

fibers are pulled out at the crack surface with the increase in applied loads. This is thought to be the reason for a higher crack load obtained for CNFRC samples, particularly SCB4.

The CNF dispersion in some parts was seen to be denser, while at other location, a single fiber was observed. The difference between the two observations reveals that the dispersion of fibers was not completely homogenous within the matrix and that a perfect single fiber distribution within the matrix was not achieved. The SEM images of core samples for SCB6, SCB7, and SCB8 are also represented in Figure 10. No CNF clump was detected for any of these samples. The presence of the CNF was also spotted adjacent to the steel fiber in the SCB6 sample. The CNF fiber seemed to be fractured in the mid-length. This could mean that the embedded CNF, in the vicinity of SF, contributed to the energy dissipation of the sample, and also it aided the SF in energy dissipation. In addition, they enhanced the performance of SF by reinforcing the matrix surrounding the steel fibers. The analysis of SEM images of specimen SCB7 shows that fibers partially filled the micro-voids. Such phenomenon would reduce the permeability by void compaction and this could result in higher compressive strength. None of the observed samples showed any CNF clumps or agglomerations.

4.3. Beam test results

The load displacement curves of all samples in the three different categories as well as the average recorded strains from the tension steel plate (G19 and G20) at midspan are depicted in Figures 11 and 12 respectively. Also, the strain results from tie bars of all specimens are presented in Figures 13-20. The overall observed behaviour of each category is described in the following subsections.

4.3.1. Category 1 test results

The load-displacement behaviour for all beams shown in Figure 11 showed almost linear response up to 80% of the maximum load. All SC beams exhibited relatively uniform vertical flexural cracks under applied four-point flexural loading. The number of cracks increased with the formation of two diagonal shear cracks on both west and east shear span of the beam as shown in Figure 21(a). The flexural cracks did not increase in length or width, while one shear crack showed gradual widening under increasing load and the load-displacement response became nonlinear. Limited number of flexural cracks and dominance of shear crack development in the beams in this category was due to the lower shear capacity of the beam compared to the flexural capacity because of insufficient amount of vertical shear reinforcement (i.e. tie bars) and inadequate concrete strength. Hence, the shear failure occurred before further flexural damage (i.e. flexural cracks). For this category, the structural damage of all SC beams was marked by a major shear crack widening on one side of the beam at the peak load (Figure 21) and by a sudden load drop on the load-displacement curve. During the post-peak stage, followed by severe increase in crack width, local buckling of the compression steel plate and concrete crushing (Figure 22) took place and the concrete core was split into two sections. Hence, only steel

plates and tie bars were contributing in resisting the applied forces until the maximum displacement limit of the testing machine was reached and the test was terminated.

The formation and subsequent opening of diagonal tension cracks in the concrete core describe the nature of a shear failure. A diagonal crack in the core can form at a relatively low load. However, it should be noted that failure does not occur until the crack has opened significantly. The significant crack opening for all samples by splitting the concrete core into two sections and rupture of tie bars (Figure 23) at the location of the shear crack signified the failure of the specimen.

SFRC showed the highest energy dissipation through yielding of the tension steel plate (Figure 12(a)). CNFRC1.0 and CNFRC0.5 for SCB4 and SCB3 respectively, performed better in delaying the formation of flexural cracks compared to PC by 29% and 6.5% respectively. All FRC in this category delayed the formation of the first shear crack compared to the control sample SCB1. Amongst all, SFRC had the highest effect followed by CNFRC1.0 and CNFRC0.5 respectively. Furthermore, CNFRC1.0 performed better than CNFRC0.5 regarding the resistance of the core against applied shear forces as less strain values were monitored on tie bars (Figure 15 and Figure 16). Having said that, the amount of fibers were insufficient to alter the failure mode of the SC beam since a shear failure was observed for all specimens.

Overall, the CNF fibers were more effective with 1.0% concentration in delaying the formation of the micro-cracks, especially the flexural cracks, while SF with 0.5% dosage was more effective in controlling the macro-size cracks and decelerating crack widening. It is evident that SF and CNF have been effective in enhancing the structural performance of the SC beam to some extent at different scales and they had different effects on the crack behaviour. This implies the need for benefiting from both improvements which can be obtained by combining the fibers within the matrix. The complementary action of nano- and micro-scale fiber reinforcement in concrete (rather than each of them individually) could render desired benefits to concrete material properties since they function at different scales. Also, according to few previous studies [19-20], it is thought that nanofibers contribute to the interfacial stress transfer from macro fibers to the cementitious matrix and they can enhance the bonding and pull-out behaviour of macro-scale fibers.

Therefore, to better observe the effect of both fibers on the structural performance of SC beams, it was aimed to use a hybrid fiber reinforced concrete combining both CNF and SF to enhance the material behaviour at two different scales and analyse their effect on the overall performance of the SC element. Accordingly, category 2 which was designed and tested to pursue this aim, is further discussed in the following section.

4.3.2. Category 2 test results

The samples in category 2 with overall 2.0% fibers showed flexure-shear failure with ductile load-displacement curve as shown in Figure 11. The crack pattern in these beams initiated with flexural cracks and further development of flexural crack length. Higher number of flexural cracks could be observed for both SCB5 and SCB6 as opposed to beams in category 1. Both beams had an elastic-plastic load-displacement curve and after reaching the ultimate load, the load resistance was governed by the shear capacity of the beam, and an increase in a single shear crack width resulted in a load drop. The beam maintained its loading capacity at about 60% of the ultimate load, but due to the limited displacement of the testing machine, the test was terminated at around a midspan displacement of 45 mm.

In comparison to category 1, both SCB5 and SCB6 showed significant tension steel plate yielding (Figure 12(b)), hence there existed a ductile mode of energy dissipation. Moreover, the width of the shear cracks after the crack opening was significantly less compared to the width of major shear cracks for the control specimen and beams in category 1. As a consequence of better crack control, category 2 showed less severe compression plate buckling, hence the overall displacement of the beam was symmetric with smaller shear deformation within a great displacement range.

Despite the higher compressive strength and tensile strength of concrete for SCB6 than SCB5, flexural cracks and shear cracks for SCB5 were further delayed during the test and they formed at a higher load level. This is because higher CNF dosage was used in SCB5 and nanofibers were bridging the nano-cracks and micro-cracks more efficiently, therefore they were effective in giving a better crack pattern to SCB5 as opposed to SCB6. When the cracks reached the macro size, steel fibers were responsible for bridging the cracks and preventing excessive crack opening, where SCB6 performed better in terms of the ultimate strength and ductility due to the higher steel fiber dosage.

Overall, the addition of 2.0% hybrid fibers to the concrete successfully altered the failure mode of the beam from diagonal tension failure to flexural-shear failure and significantly improved the ductility of the SC element. This was due to the increased shear capacity of the concrete core. To further investigate the effect of lower fiber concentration, which is more desirable in terms of cost and concrete weight, and whether the ductile failure mode observed for category 2 could be achieved with less fiber concentration, the overall fiber concentration of 1.5% was investigated. Category 3 SC beams were tested to investigate whether their response would be in any way superior or different to that of category 2.

4.3.3. Category 3 test results

The load-displacement curve for this category is shown in Figure 11. The crack pattern for both beams were following similar progression stages in which initial vertical flexural cracks appeared,

followed by a short diagonal hairline crack in the shear span. The occurrence of several flexural cracks also increased the magnitude of the longitudinal strains measured in the steel faceplates (Figure 12(b)). At the hardening stage of the load-displacement curve, the length and width of flexural cracks were increasing while at the ultimate load, one shear crack showed an increase in width resulting in negative stiffness and a reduction of the loading capacity of the beam.

Despite similar trend observed for the crack behaviour of both beams; SCB8 had a lower shear capacity which is attributed to lower steel fiber dosage of this beam against SCB7. At V_f of 1.0% SF, the concrete core performed better in controlling the macro-size crack propagation at higher load level. The bridging effect of steel fibers is shown in Figure 24. On the other hand, it is interesting to note that the formation of the initial flexural and shear cracks was further delayed in SCB8. This was due to the effect of higher V_f of nanofibers. Furthermore, the strain induced on tie bars within the shear span with minor shear crack, was lower for beams with higher CNF dosage, which signifies the effect of CNF on the structural performance by micro-crack bridging. Overall, both beams were successful in altering the shear failure mode of the control beam with plain concrete core into a ductile mode of failure.

4.3.4. Comparison of all samples

To compare the results for all eight samples, the results were normalized as shown in Figure 11. To normalize the load-displacement curves, the total applied load (P) was divided by the concrete compressive strength at 28 days (f'_c). The displacement was normalised as D/L, where D is the mid-span deflection and L is the span length. Summary of the results obtained from load-displacement curves for all eight SC beams is also detailed in Table 6.

From Figure 11, it can be seen that CNFRC1.0 performed better than other specimens amongst singly-reinforced FRC samples with higher strength and higher energy dissipation. Amongst hybrid fiber reinforced samples, those with higher V_f of macro fiber showed better ductility, while the strength of samples with less steel fibers was maintained due to the combined effect of nanofibers and macro fibers.

For the control specimen, flexural cracks appeared at early stages of loading, i.e., about 11% of the shear force capacity of the specimens. This early flexural cracking indicates the relatively quick transition from uncracked to cracked section, which is important to consider in structure stiffness evaluation.

The control sample, as well as beams in category 1, failed in a shear mode. For these SC beams, cracks normally appeared first at the moment span in the extreme lowest fiber of the concrete core. They only showed few number of cracks, short in length, which were formed as flexure cracks. Shear cracks appeared following the flexural cracks. The onset of the major diagonal shear crack opening

was observed at the peak load resulting in negative stiffness for the beam. Soon after the load drop, the shear crack widened and the core split in two sections. For SCB2, the macro steel fibers were found to be ineffective in delaying the initiation and progression of macro cracks, which can be due to the relatively large spacing between fibers. A critical factor for the control beam and those in category 1 with shear failure was the inadequate tensile strength of concrete, which was exceeded in the principal direction at the maximum load obtained on the curve. The ductility of this category was less than other categories.

On the other hand, there was evidence of good curvature formed during the test and a good deal of ductility in the behaviour of beams in category 2 and category 3. The load-displacement responses indicate that both categories had elastic-plastic behaviour with significant displacement ductility due to flexural yielding of the tension steel plate, and the overall tie bar strains were small and much smaller than those in category 1. All beams in these two categories began to display rapid loss of stiffness corresponding to tension steel plate yielding. For beams with hybrid FRC concrete core, at the ultimate load as well as flexural yielding of the tension (bottom) steel plate, the concrete was still contributing in resisting load due to the presence of steel fibers; therefore, the ultimate resistance was governed by both concrete and steel plates.

By comparing the results for SCB8 (SF0.5%+CNF1.0%), SCB2 and SCB4, it can be seen that there has been a significant enhancement in ductility of the beam for SCB8 owing to the combined action of both fibers. As experimentally investigated by Wright et al. [21], the low concrete compression strength did not change the fundamental failure mode of the double skin composite beams under four-point bending but only the level at which failure occurred. It can be emphasised that for SC beams in category 2 and category 3 with less concrete compressive strength than control specimen, which showed different failure mode, the change in the failure mode was strictly due to the presence of fibers.

From Table 6, it can be concluded that 1.0% CNF was successful in delaying the formation of the shear cracks by the act of bridging nano-cracks and micro-cracks. The evidence for this observation comes from the comparison of the load at first concrete shear crack ($P_{s,crack}$) for both categories 2 and 3 in which the beam with 1.0% of CNF in each category showed higher load level. The shear force margin between the appearance of the flexural crack and brittle shear crack was at its maximum for SCB5.

The effectiveness of the CNF as flexural reinforcement was more pronounced for singly-reinforced FRC core (category 1), as opposed to shear reinforcement. The mechanism of the CNF within the concrete as Konsta-Gdoutos et al. [17] also described, is that they enhance the material's ability to control the coalescence of cracks at the nano-scale and the subsequent formation of micro-cracks, hence a higher amount of energy is required to initiate cracking. Also, damage localisation is avoided

by fibers arresting crack growth upon the initiation of matrix cracking; thereby, 'energy is dissipated through the formation of a dense field of micro-cracks (with widths less than 100 μm)' [22].

This observation is confirmed by the comparison between the load at first concrete flexural crack ($P_{f,crack}$) of SCB4 and other beams, in which 1.0% CNF had the highest enhancement with 29% increase in initial flexural crack load. While the greatest effect on the initial shear crack formation was recorded for SCB2 with 0.5% steel fibers. The load at which initial flexural crack occurred for SCB8 was higher than SCB7, which could be attributed to higher CNF concentrations; however, in category 2, for SCB6 with 1.5% of steel fibers the initial flexural crack appeared at 26.3% of the ultimate load and this phenomenon occurred at 25% of the ultimate load for SCB5. This could be due to the high steel fiber dosage that has had a slight effect on the load level. From another viewpoint, SCB6 had the highest w/c ratio due to the high volume fraction of fibers and it had the lowest slump, and the handling and compacting of the concrete in the structural element was very difficult and hence the chance of fiber interlocking is increased. Also, the density of this concrete (Figure 9) was the highest amongst all. In the construction industry, concrete which has good workability (e.g. self-consolidating concrete) and has lower weight (e.g. lightweight concrete) are more desirable especially for structures that use SC system, in which the consolidation of the concrete could be challenging. Therefore, this could be a drawback for beam SCB6 which could increase the weight of the structure especially in massive structural elements, thus it would be less practical for SC applications. Furthermore, the shearing deformation for beams in categories 2 and 3 was less than those in category 1.

In terms of load capacity of the beams, there is limited literature on the effect of fibers on SC beams. However, in review of the available results from past studies, Liew and Soheli [23] studied the addition of PVA fibers to the SC beams with J-hook connectors and they showed that the load carrying capacity was increased by 25%. In this research study, in a descending order, the load carrying capacity was enhanced by 48.5%, 46.2%, 39.4%, 35.6%, and 13.1% for SCB6, SCB7, SCB5, SCB8 and SCB2 respectively, which was greater than the aforementioned research finding.

Figure 25 shows the crack map for all eight SC beams. From the figure, it is evident that the number of flexural cracks increased for category 2 and category 3 beams which had hybrid FRC core. Also, the shear crack at the end of the test had greater width for beams in category 1, because the use of hybrid fibers especially with SF dosage higher than 0.5%, was more effective in controlling crack width. Within category 1, SCB4 showed more cracks with less spacing along the span than other singly-reinforced beams and SCB1. This shows a better flexural crack distribution with higher CNF fibers.

For the beams with a hybrid core, SCB5 showed more cracks distributed along the length (with less crack spacing), while for SCB6 the width of flexural cracks was larger than those in SCB5. Also, SCB7 showed higher flexural crack width than SCB8, while SCB8 developed more cracks. This

observation provides a deeper insight into the contribution of higher CNF dosage in giving more crack distribution, while higher SF dosage helps with energy dissipation through increased crack width.

These results imply that using hybrid fibres can greatly improve the material performance of concrete girders. Further experimental work is suggested to be conducted to find the optimum CNF/SF mixture ratios, and further hybrid combinations are suggested to be investigated.

5. Conclusions

To conclude the findings of the experimental investigation carried out in this paper, the effect of each fiber type and their performance in combination with the second fiber type is outlined. The material mechanical properties' test results of the 1.0% CNF concrete did not show much improvement, which could have been due to presence of clumps at concrete sections that were not observed.

The beam test results indicated that steel fibers used in this study enhanced the shear capacity of the beam after initial cracking, hence improving the ductility at the post-peak stage; while during the early stages of loading, nanofibers provided the material with the ability to carry a higher load as well as to improve the performance throughout the entire loading phase (which was attained through enhanced C-S-H and interfacial interaction of fibers). The initial performance was best improved for each category as follows.

Category 1: 1.0% CNF showed the best results in delaying the formation of both initial flexural cracks and shear cracks.

Category 2: 1.0% CNF combined with 1.0% SF showed better performance in delaying the formation of initial shear crack, while the initial flexure crack was controlled at similar load level as concrete with 0.5% CNF and 1.5% SF.

Category 3: 1.0% CNF showed the best result in delaying the formation of both initial flexural cracks and shear cracks.

It is concluded that 1.0% CNF showed a good effect on the performance of the beam, both in singly reinforced concrete as well as in combination with SF. The experimental investigation carried out showed that the combination of nano (CNF) and macro size fibers (SF) improved the structural response, both for category 2 beams ($V_f = 1.5\%$) and category 3 beams ($V_f = 2.0\%$), so much that an adequate content of fibers could change the failure mode from shear to flexure-shear. In this research, the optimum hybrid fiber ratio was found to have a minimum of 0.5% steel fibers and minimum overall 1.5% volume fraction of fibers. Moreover, it was found that the strain induced on tie bars was minimised as opposed to the control sample, while the strain induced on the steel plates was maximised. The combination of fibers at two scales, provided a delay in the formation of cracks and

higher post cracking stiffness because of a better crack-arresting mechanism and higher tension stiffening of the concrete. It should be noted that due to better crack control at the macro scale, other shear resisting mechanism of the concrete namely the aggregate interlock, is improved, providing more shear resisting capacity. The brittle failure of the concrete core was prevented and large flexural deflection range (28-38mm) without severe plate deformation (i.e. shear deformation) was obtained.

To conclude, the use of an overall V_f of 1.5% is recommended for the design of SC with FRC concrete core as opposed to 2% since this category proved to be sufficient to alter the failure mode of the beam and achieve a high ductility and energy dissipation. This amount is subjected to the use of a minimum of 0.5% of steel fibre in combination with nanofibers. Using less fiber content in the structural element is preferred due to better workability as well as less self-weight of the concrete. On the other hand, the use of higher CNF content in the hybrid fiber reinforced concrete (e.g. SCB5 & SCB8) is recommended, if one wish to obtain better self-health monitoring properties within the structural element, an issue that will be extensively discussed in another paper.

Acknowledgments

The first author is grateful to the financial support obtained by City, University of London. The authors wish to thank the technical staff of the Structural Laboratory at City, University of London. The authors would also like to thank Queen Mary University for allowing them to use their Scanning Electron Microscope.

References

- [1] Liew, J.Y.R., Soheli, K.M.A. and Koh, C.G. (2009). Impact tests on steel-concrete-steel sandwich beams with lightweight concrete core. *Engineering Structures*. 31, 2045-2059.
- [2] Takeuchi, M., Narikawa, M., Matsuo, I., Hara, K. and Usami, S. (1998). Study on a concrete filled structure for nuclear power plants. *Nuclear Engineering and Design*. 179 (2), 209-223.
- [3] Oduyemi, T.O.S. and Wright, H.D. (1989). An Experimental Investigation into the Behaviour of Double-Skin Sandwich Beams. *Journal of Construction Steel Research*. 14 (3), 197-220.
- [4] Wright, H.D., Oduyemi, T.O.S. and Evans, H.R. (1991). The Experimental Behaviour of Double Skin Composite Elements. *Journal of Constructional Steel Research*. 19 (2), 97-110.
- [5] Sanchez, F. and Ince, C. (2009). Microstructure and macroscopic properties of hybrid carbon nanofiber/silica fume cement composites. *Composites Science and Technology*, vol. 69, no. 7-8, pp. 1310-1318.
- [6] Yazdanbakhsh, A., Grasley, Z., Tyson, B., and Abu Al-Rub, R. (2009). Carbon Nano Filaments in Cementitious Materials: Some Issues on Dispersion and Interfacial Bond. *Nanotechnology of Concrete: The Next Big Thing Is Small*.
- [7] Yazdanbakhsh, A., Grasley, Z., Tyson, B., and Abu Al-Rub, R. (2010). Distribution of Carbon Nanofibers and Nanotubes in Cementitious Composites. *Journal of the Transportation Research Board, Transportation Research Board of the National Academies*, no. 2142, 89-95.
- [8] Camacho-Ballesta, C., Garces, O., and Zornoza, E. (2016). Performance of cement based sensors with CNT for strain. *Advanced Cement Research*, vol. 28, no. 4, 274-284.
- [9] Tyson, B., Abu Al-Rub, R., Yazdanbakhsh, A., and Grasley, Z. (2011). Carbon Nanotubes and Carbon Nanofibers for Enhancing the Mechanical Properties of Nanocomposite Cementitious Materials. *Journal of Materials in Civil Engineering*, vol. 23, no. 7, 1028–1035.
- [10] Metaxa, Z., Konsta-Gdoutos, M. and Shah, S. (2013). Carbon nanofiber cementitious composites-effects of debulking procedure on dispersion and reinforcing efficiency. *Cement and Concrete Composites*, no. 36, 25-32.
- [11] Yazdani, N. and Mohanam, V. (2014). Carbon Nano-Tube and Nano-Fiber in Cement Mortar: Effect of Dosage Rate and Water-Cement Ratio. *International Journal of Material Science (IJMSCI)*, vol. 4, no. 2, 45-52.
- [12] Gao, D., Sturm, M. and Mo, Y. (2009). Electrical resistance of carbon-nanofiber concrete,” *Smart Materials and Structures*, vol. 18.
- [13] Sivakumar, M. (2011). Performance characteristics of Carbon Nanofiber Blended Self Compacting Concrete. *International Journal of Advanced Structural Engineering*, vol. 3, no. 2, 179-186.
- [14] Howser, R.r., Dhonde, H. and Mo, Y. (2011). Self-sensing of carbon nanofiber concrete columns subjected to reversed cyclic loading. *Smart Materials and Structures*, no. 20, 1-13.

- [15] Yazdanbakhsh, A. (2012). *Production, Characterization, And Mechanical Behavior of Cementitious Materials Incorporating Carbon Nanofibers*. PhD thesis. Texas A&M University. Texas.
- [16] Kim, H., Nam, I. and Lee, H. (2014). Enhanced effect of carbon nanotube on mechanical and electrical properties of cement composites by incorporation of silica fume. *Composite Structures*, no. 107, 60-69.
- [17] Konsta-Gdoutos, M.S., Metaxa, Z.S. and Shah, S.P. (2010). Highly dispersed carbon nanotube reinforced cement based materials. *Cement and Concrete Research*. 40 (7), 1052-1059.
- [18] Mo, Y.L. and Howser Roberts, R. (2013). Advances in Nanofibers. In: Maguire, R. (Ed.) *Carbon Nanofiber Concrete for Damage Detection of Infrastructure*. InTech. pp.125-143. Available from: <https://www.intechopen.com/books/advances-in-nanofibers/carbon-nanofiber-concrete-for-damage-detection-of-infrastructure> [Accessed 1st December 2015].
- [19] Peyvandi, A., Sbiya, L.A., Soroushian, P. and Sobolev, K. (2013). Effect of the cementitious paste density on the performance efficiency of carbon nanofiber in concrete nanocomposites. *Construction and Building Materials*, 48, 265-269.
- [20] Willie, K. and Loh, K.J. (2010). Nanoengineering Ultra-High-Performance Concrete with Multiwalled Carbon Nanotubes. *Journal of the Transportation Research Board*. 2142, 119-126. Available from: DOI: 10.3141/2142-18 [Accessed 15th April 2013].
- [21] Wright, H.D., Oduyemi, T.O.S. and Evans, H.R. (1991). The Experimental Behaviour of Double Skin Composite Elements. *Journal of Constructional Steel Research*. 19 (2), 97-110.
- [22] Hou, T.C. and Lynch, J.P. (2005). Conductivity-based strain monitoring and damage characterization of fiber reinforced cementitious structural components. In: *Proceedings of SPIE 12th Annual International Symposium on Smart Structures and Materials, San Diego, CA, March 6-10*. Available from: <http://www-personal.umich.edu/~jerlynch/papers/SPIE2005Conductivity.pdf> [Accessed 14 October 2015].
- [23] Liew, J.Y.R. and Sohel, K.M.A. (2009). Lightweight steel-concrete-steel sandwich system with J-hook connectors. *Engineering Structures*. 31, 1166-1178.

Parameter	Dimension	Description of the parameter
B	120	Plate width (mm)
t_p	5	Plate thickness (mm)
h_c	220	Concrete core thickness (mm)
t_{sc}	230	Overall SC thickness = $h_c + (2 \times t_p)$ (mm)
s	180	Stud spacing (mm)
S	180	Tie bar spacing (mm)
ρ	4.3%	Reinforcement ratio = $2t_p/t_{sc}$
d_{stud}	10	Diameter of shear stud (mm)
L_{stud}	80	Length of shear studs (mm)
d_{bar}	6	Diameter of tie bar (mm)
f_{ys}	309	Yield strength of steel plate (MPa)
$\epsilon_{y-plate}$	1545	Yield strain of the steel plates ($\mu\epsilon$)
Plate elongation	35%	Plate elongation
f_{us}	457	Ultimate strength of steel plate (MPa)
f_{y-stud}	350	Yield strength of shear stud (MPa)
f_{u-stud}	450	Ultimate strength of shear studs (MPa)
f_{y-bar}	385	Yield strength of tie bars (MPa)
f_{u-bar}	495	Ultimate strength of tie bars (MPa)
ϵ_{y-bar}	1925	Yield strain of the tie bars ($\mu\epsilon$)
Tie bar elongation	15%	Tie bar elongation

Table 1: SC beam design parameters

	SiO ₂	Retention on 45 μ m sieve	Bulk Density (Undensified) (Kg/m ³)	Specific surface (m ² /g)	Mean particle size (μ m)
Silica Fume (Elkem 940U)	> 90%	< 1.5%	200-350	15-30	0.15

Table 2: Properties of silica fume

Fiber properties	Length (l)	Diameter (d)	Aspect ratio (l/d)	Tensile strength	Young's Modulus
End-hooked steel fiber	35 mm	0.55 mm	65	1800 MPa	200 GPa

Table 3: End-hooked steel fiber properties

Fiber type	Fiber name	Average Diameter (nm)	Average length (μm)	Surface area (m^2/gm)	Dispersive Surface Energy (mJ/m^2)	Bulk Density (Kg/m^3)
CNF	Pyrograf-III PR-19-XT-LHT	150	50-200	20-30	120-140	16-48

Table 4: Properties of CNF - PR-19-XT-LHT

SC Beam Sample	Fiber				HRWR (kg)	CA (kg)	FA (kg)	Binder (B)		W/B	Slump (mm)
	SF		CNF					C (kg)	Silica Fume (kg)		
	V_f (%)	kg	V_f (%)	kg							
SCB1	-	-	-	-	2	918	955.5	360	36	0.30	80
SCB2	0.5	39	-	-	2	918	955.5	360	36	0.30	30
SCB3	-	-	0.5	1.26	2	918	955.5	360	36	0.29	90
SCB4	-	-	1.0	2.5	2	918	955.5	360	36	0.29	95
SCB5	1.0	78	1.0	2.50	2	918	955.5	360	36	0.32	46
SCB6	1.5	117	0.5	1.26	2	918	955.5	360	36	0.39	54
SCB7	1.0	78	0.5	1.26	2	918	955.5	360	36	0.32	50
SCB8	0.5	39	1.0	2.5	2	918	955.5	360	36	0.32	40

Notation: B: binder (cement + silica Fume), CA=coarse aggregate, FA= fine aggregate, C=Cement, CNF= carbon nanofiber, HRWR= high range water reducer, W= water.

Table 5: Mix proportions for SC beam samples (per m^3 of concrete)

Beam sample	Concrete type	$P_{f.crack}^*$ (kN) (% of P_{max})	$P_{s.crack}^{**}$ (kN) (% of P_{max})	P_{max} (kN)	D_u^{***} (mm)	Failure mode
SCB1 Control Sample	PC	18.8 (11.1%)	100.2 (59%)	169.6	7.6	Vertical Shear
						Diagonal shear crack
Category 1	SCB2	SFRC 0.5 33.6 (17.5%)	137 (71.4%)	191.9	7.4	Vertical Shear
						Diagonal shear crack
	SCB3	CNFRC0.5 25.5 (19.4%)	82 (62.3%)	131.6	6.5	Vertical Shear
						Diagonal shear crack
SCB4	CNFRC1.0 48.9 (29.0%)	101 (59.8%)	168.8	7.7	Vertical Shear	
					Diagonal shear crack	
Category 2	SCB5	SF1.0 + CNF1.0 59.1 (25%)	170.0 (71.9%)	236.5	28.1	Flexure-shear
						Tension steel plate yielding followed by shear crack
	SCB6	SF1.5 + CNF0.5 66.2 (26.3%)	160.0 (63.5%)	251.9	38.18	Flexure-shear
						Tension steel plate yielding followed by shear crack
Category 3	SCB7	SF1.0 + CNF0.5 56.1 (22.6%)	161 (65.3%)	247.9	35.9	Flexure-shear
						Tension steel plate yielding followed by shear crack
	SCB8	SF0.5 + CNF1.0 68.8 (30%)	169.2 (72.3%)	230	28.4	Flexure-shear
						Tension steel plate yielding followed by shear crack

*Load at the first concrete flexural crack

**Load at the first concrete core shear crack

*** Displacement at ultimate load

Table 6: Summary of test results for SCB1-SCB8

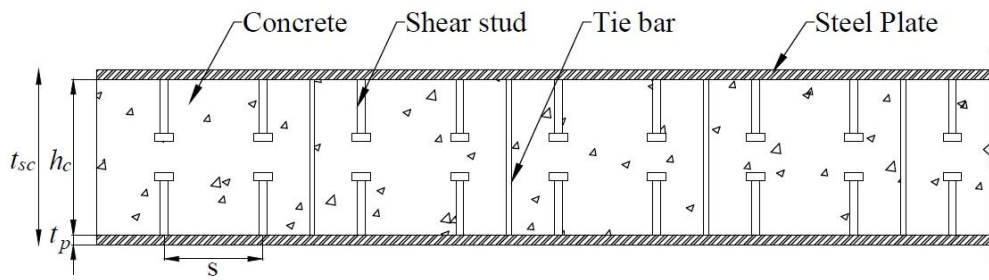


Figure 1: Schematic illustration of SC wall section

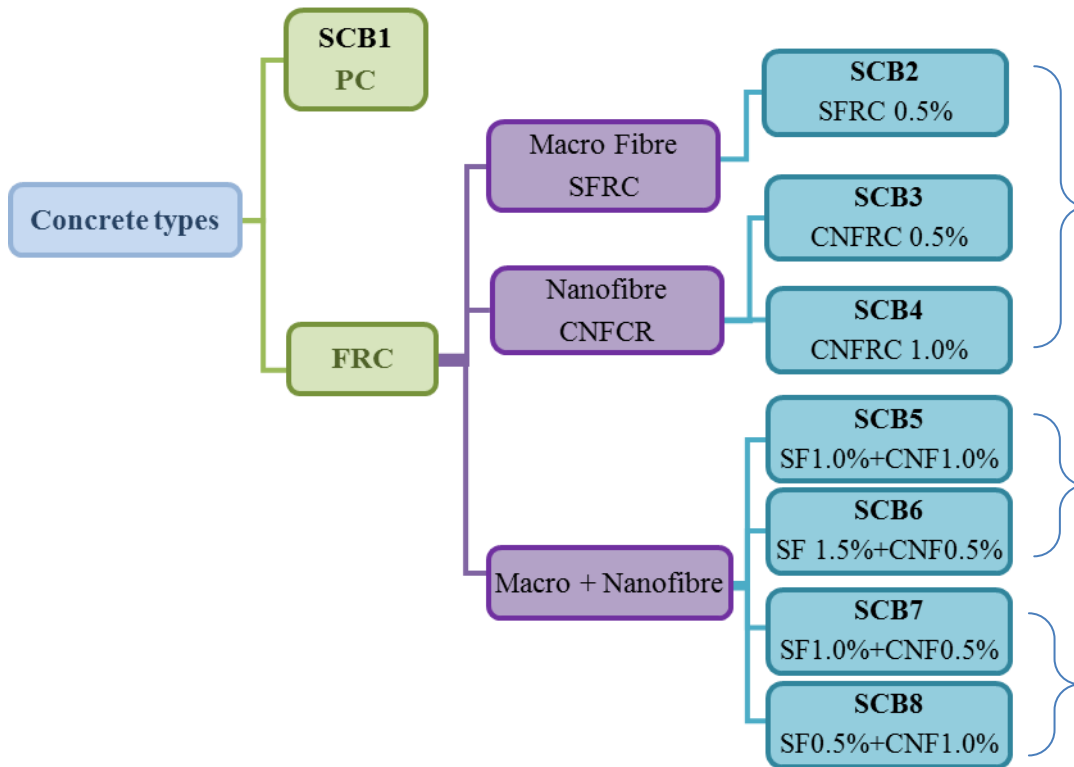


Figure 2: Concrete types used for SC beam experiments

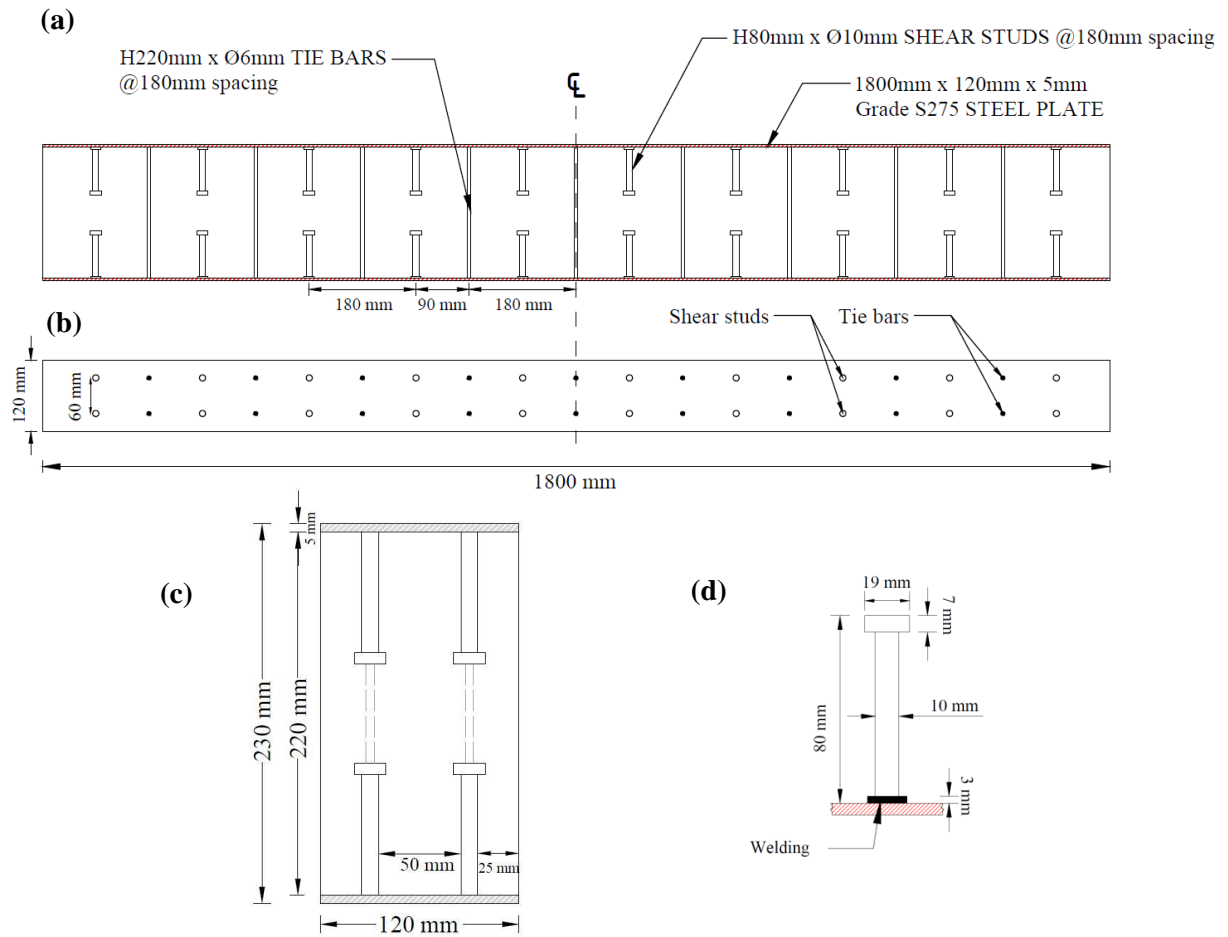


Figure 3: SC beam dimensions: (a) SC beam elevation; (b) shear stud and tie bar layout on both steel plates; (c) SC beam section; (d) shear stud details

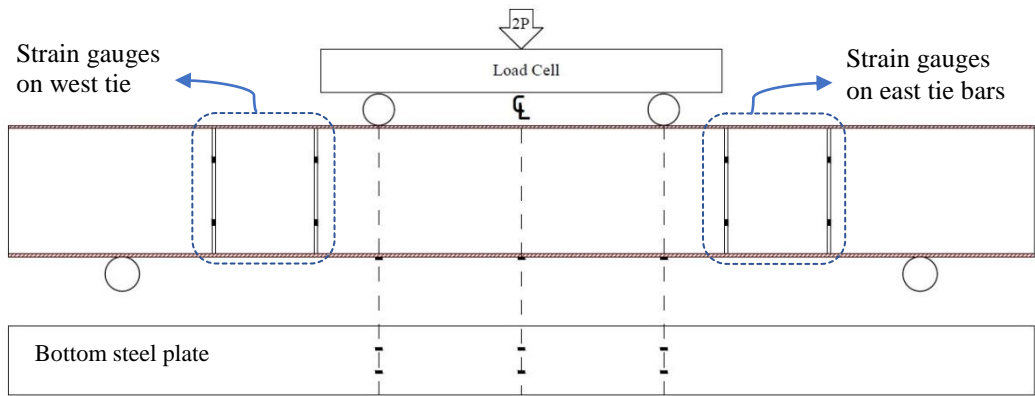


Figure 4: Location of steel strain gauges

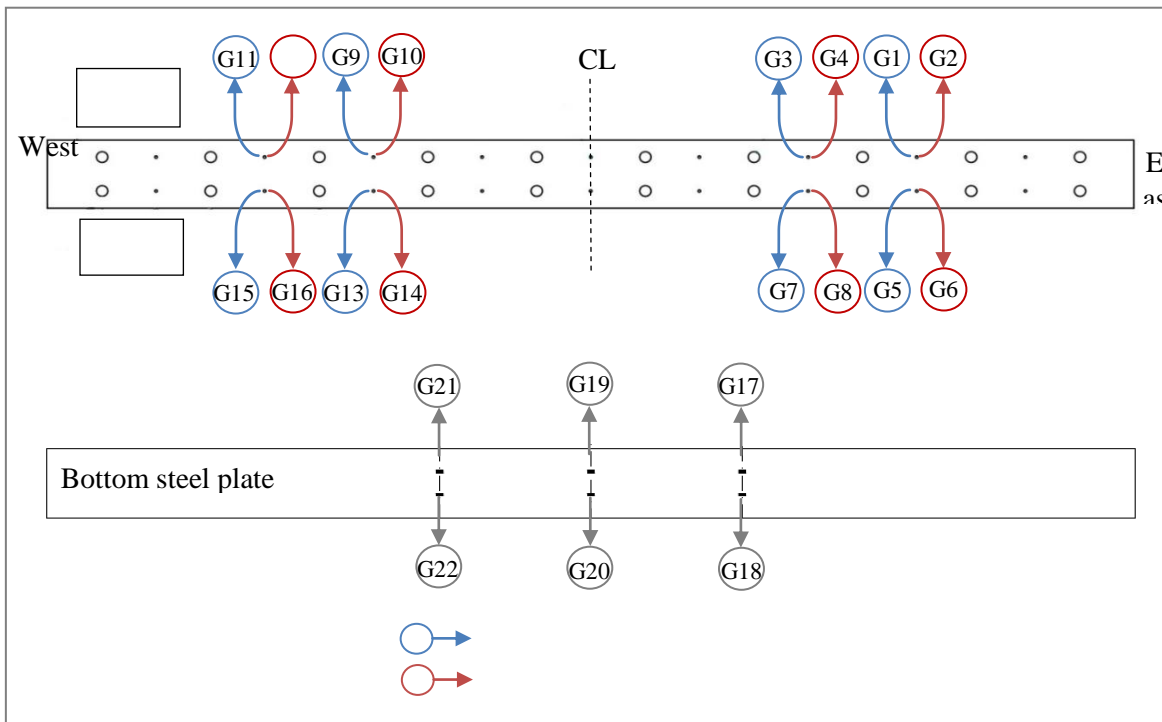


Figure 5: Strain gauge wire numbering map

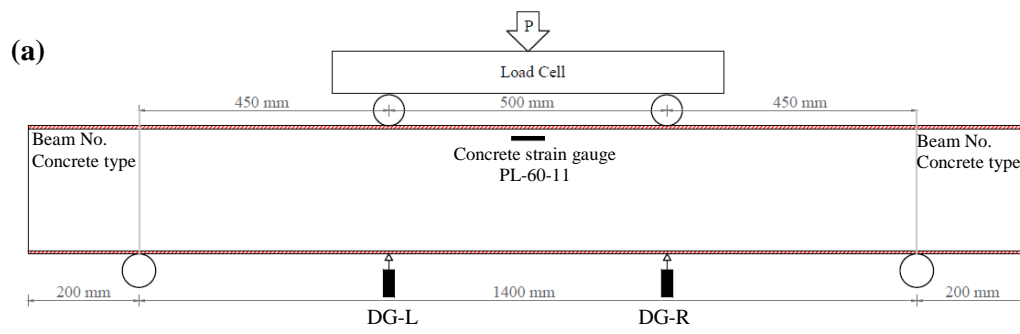


Figure 6: SC beam four-point bending test set-up: (a) schematic illustration; (b) experiment set-up

COMPRESSIVE STRENGTH (MPA)

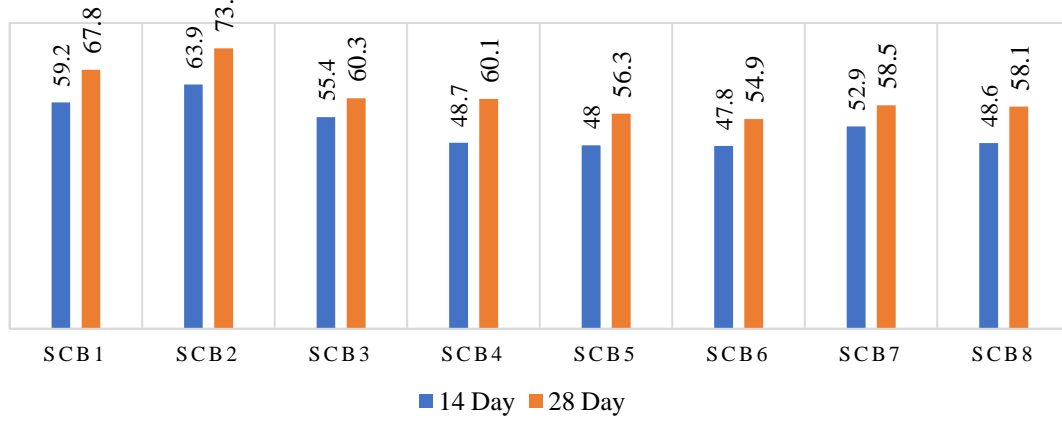


Figure 7: Concrete cube compressive strength at 14d and 28d for SCB1-SCB8

SPLIT TENSILE STRENGTH (MPA)

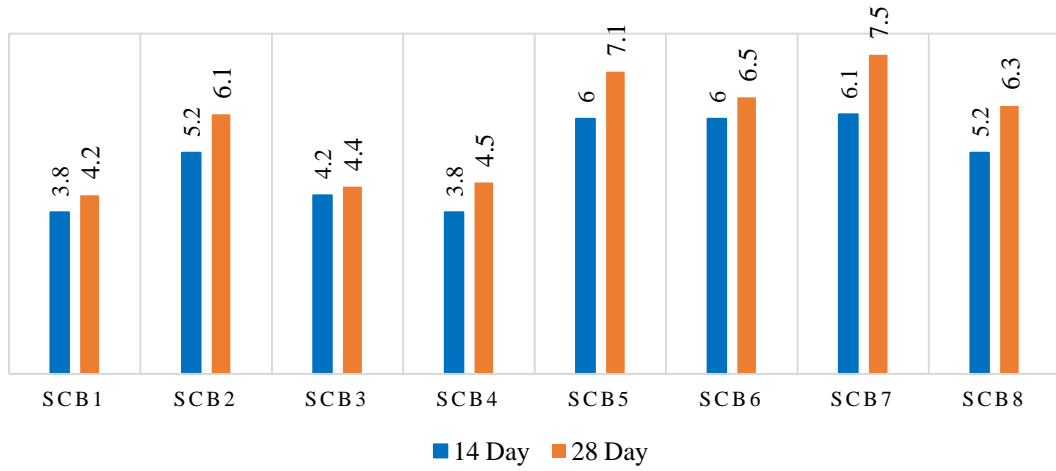


Figure 8: Concrete split tensile strength at 14d and 28d for SCB1-SCB8

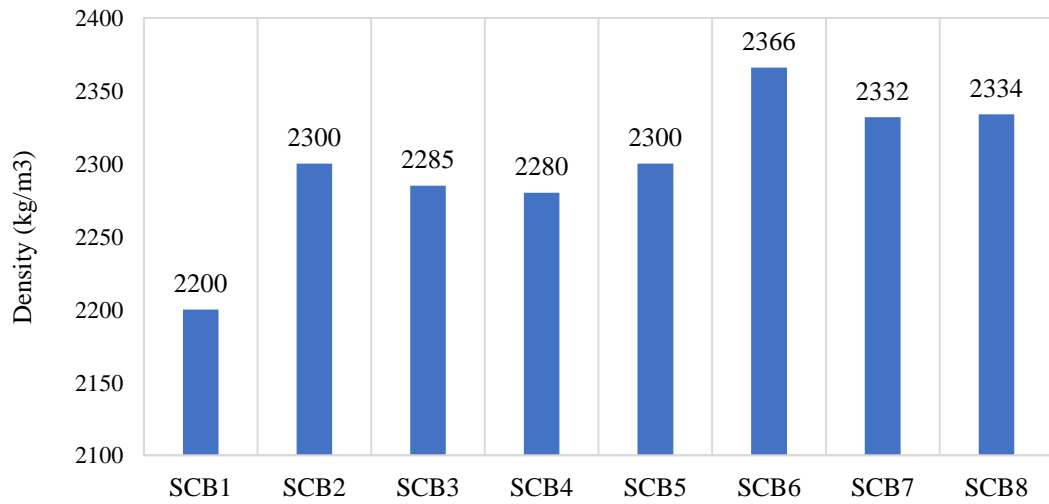


Figure 9: Concrete density for SCB1-SCB8

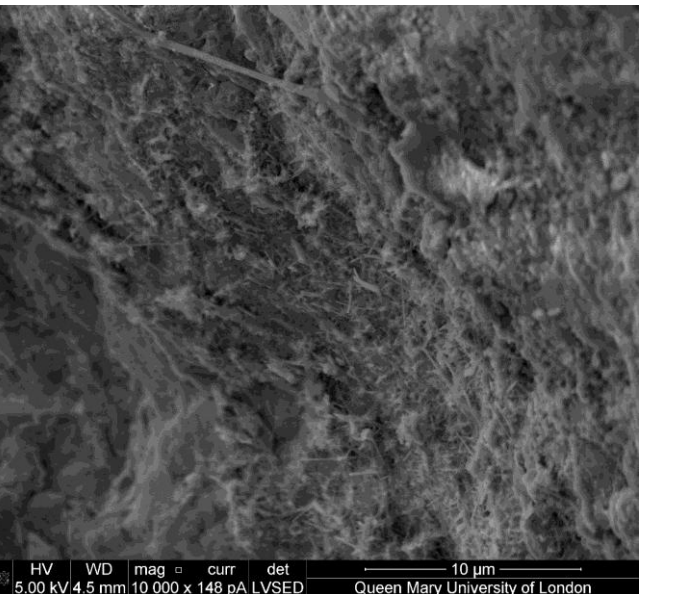
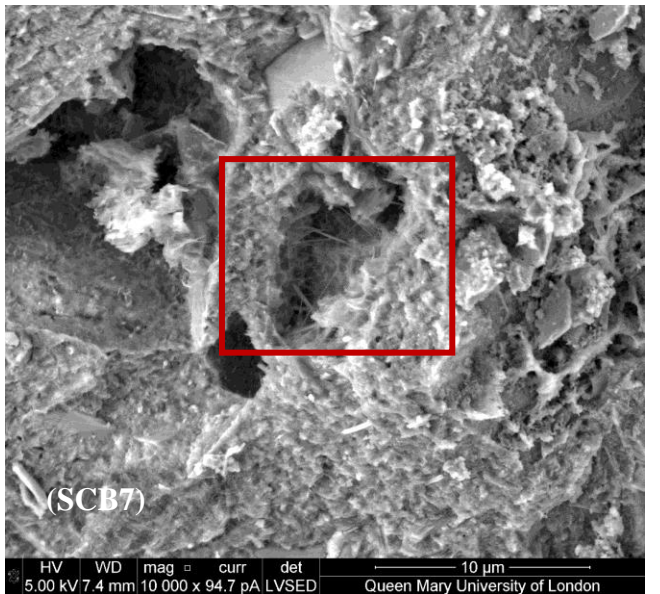
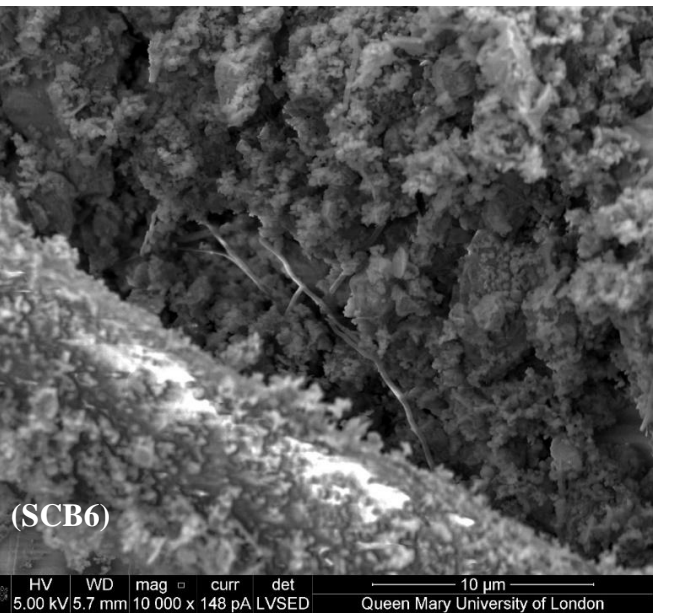
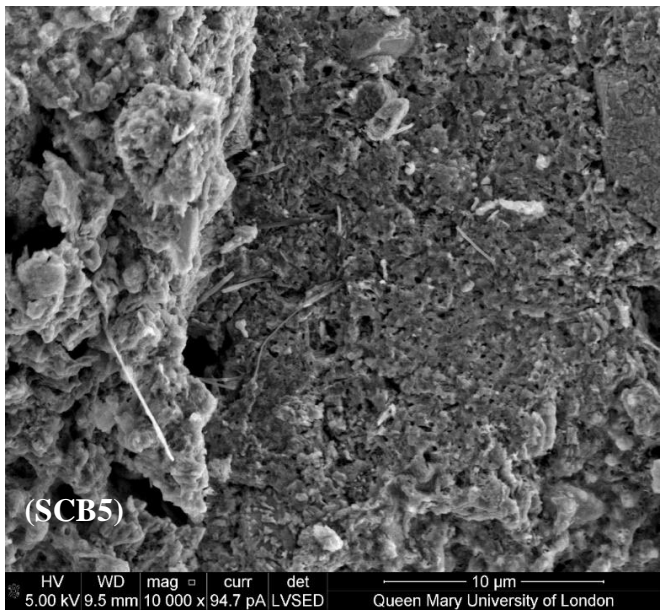
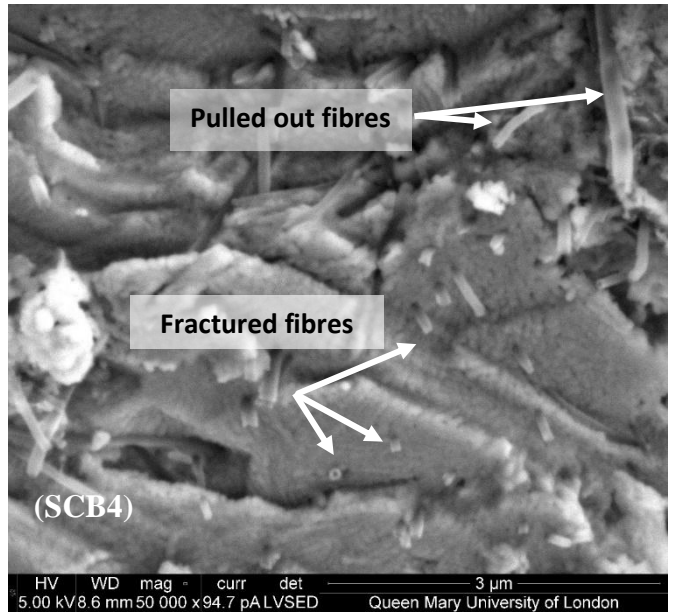
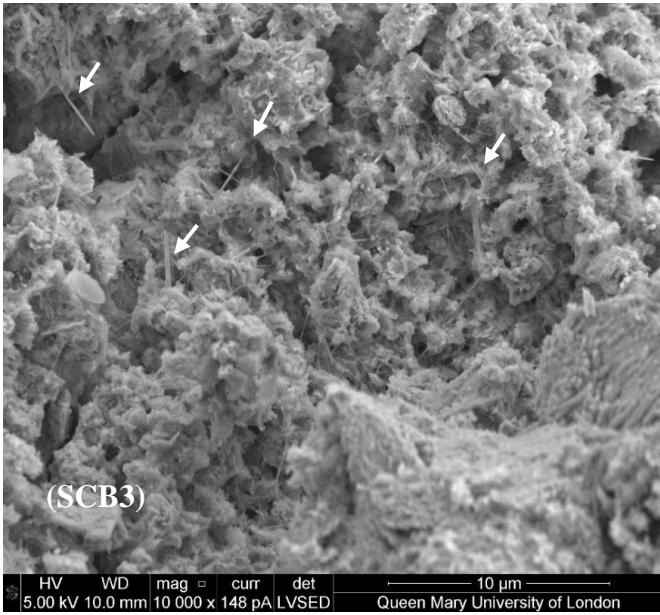


Figure 10: SEM micrographs of SCB3 - SCB8 core sample at 10000 \times magnification

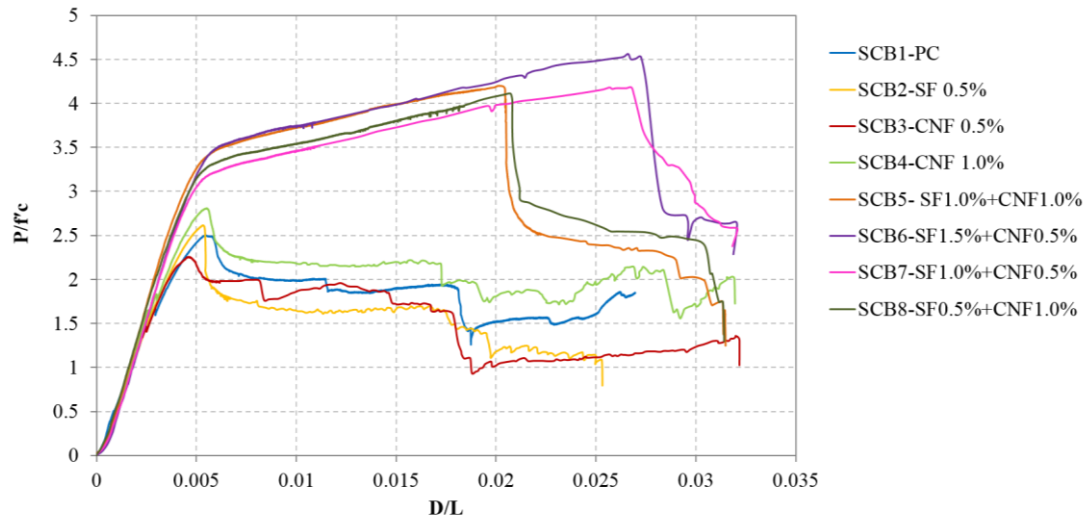


Figure 11: Normalised load-displacement curve for all tested SC beams under four-point bending

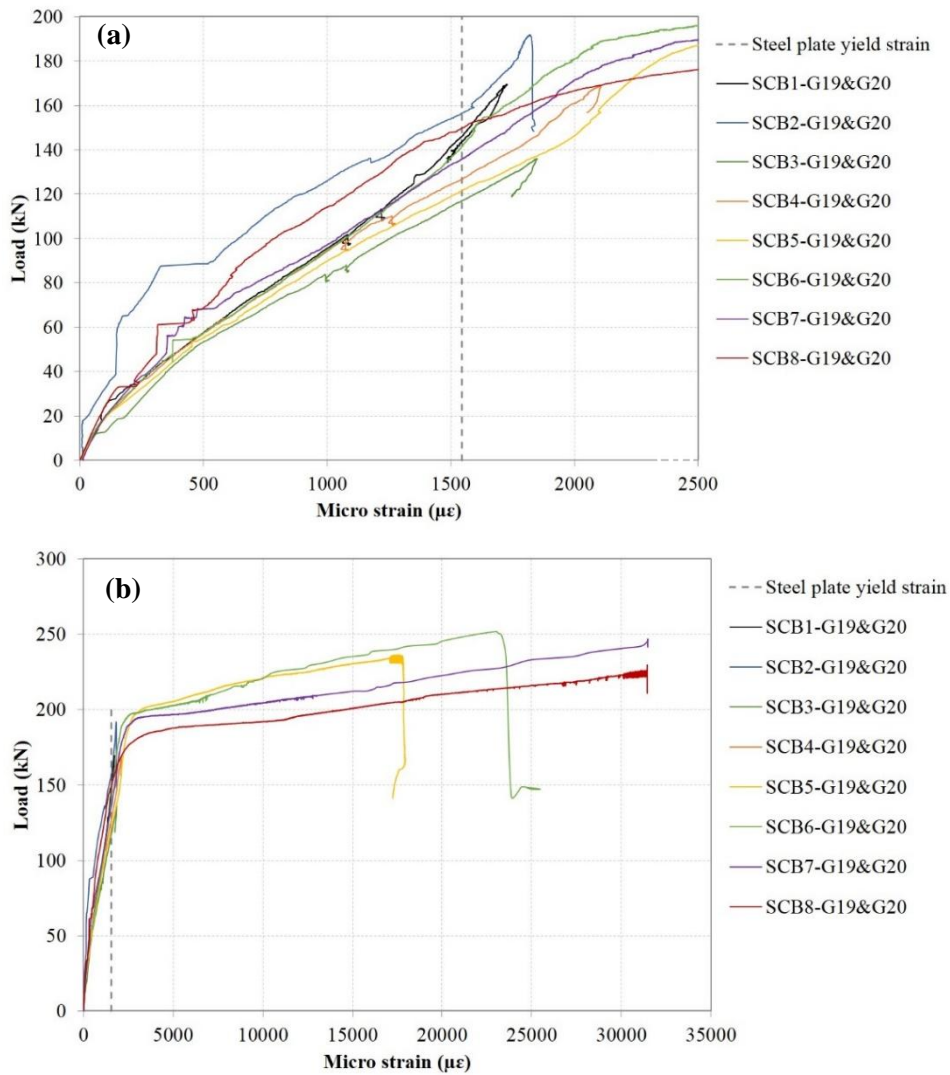


Figure 12: Average strain gauge results from bottom steel plate at midspan: (a) graph showing initial strain range up to 2500 $\mu\epsilon$; (b) Overall graph

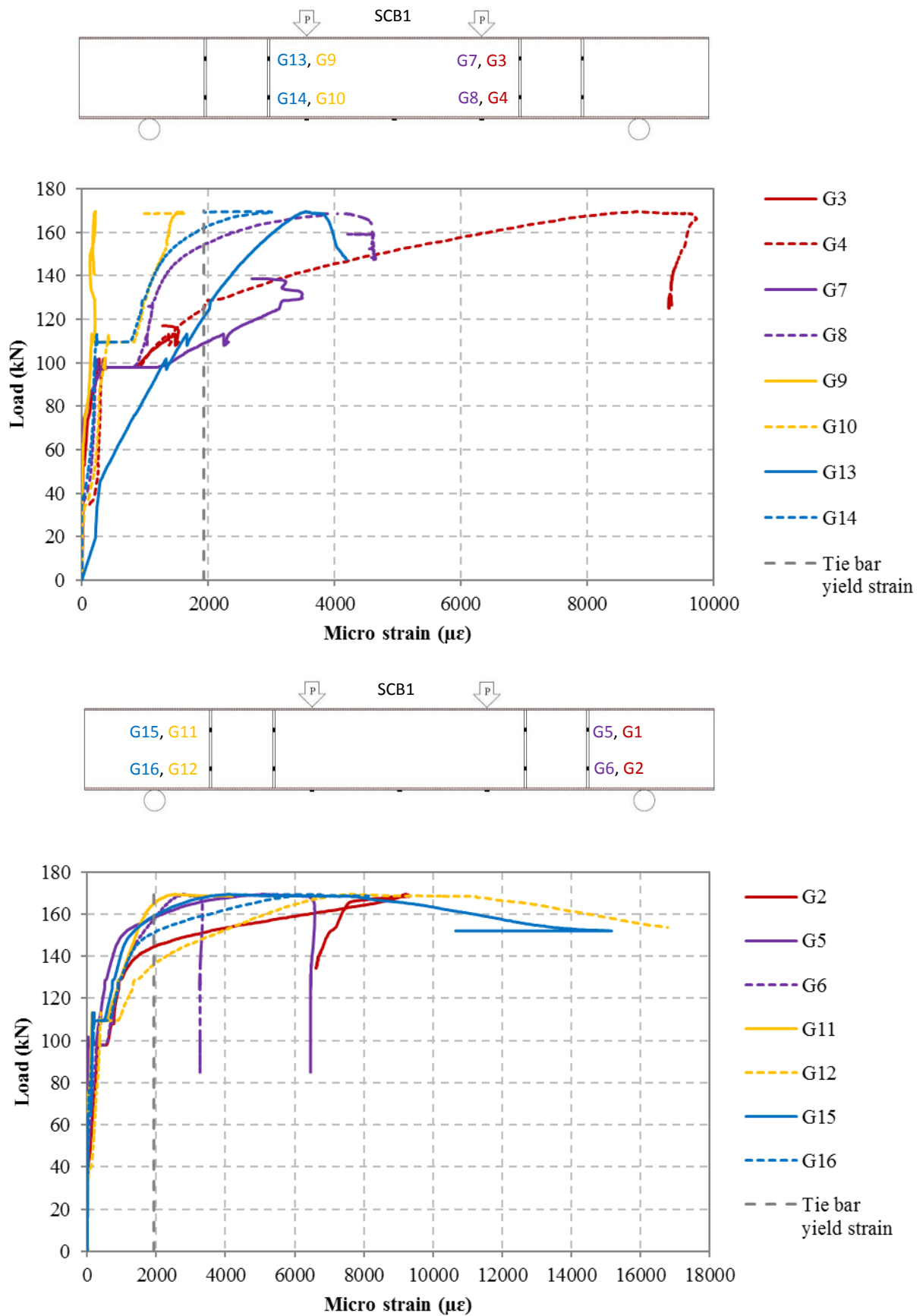


Figure 13: Measured strain for: (a) inner tie bars; (b) outer tie bars for SCB1

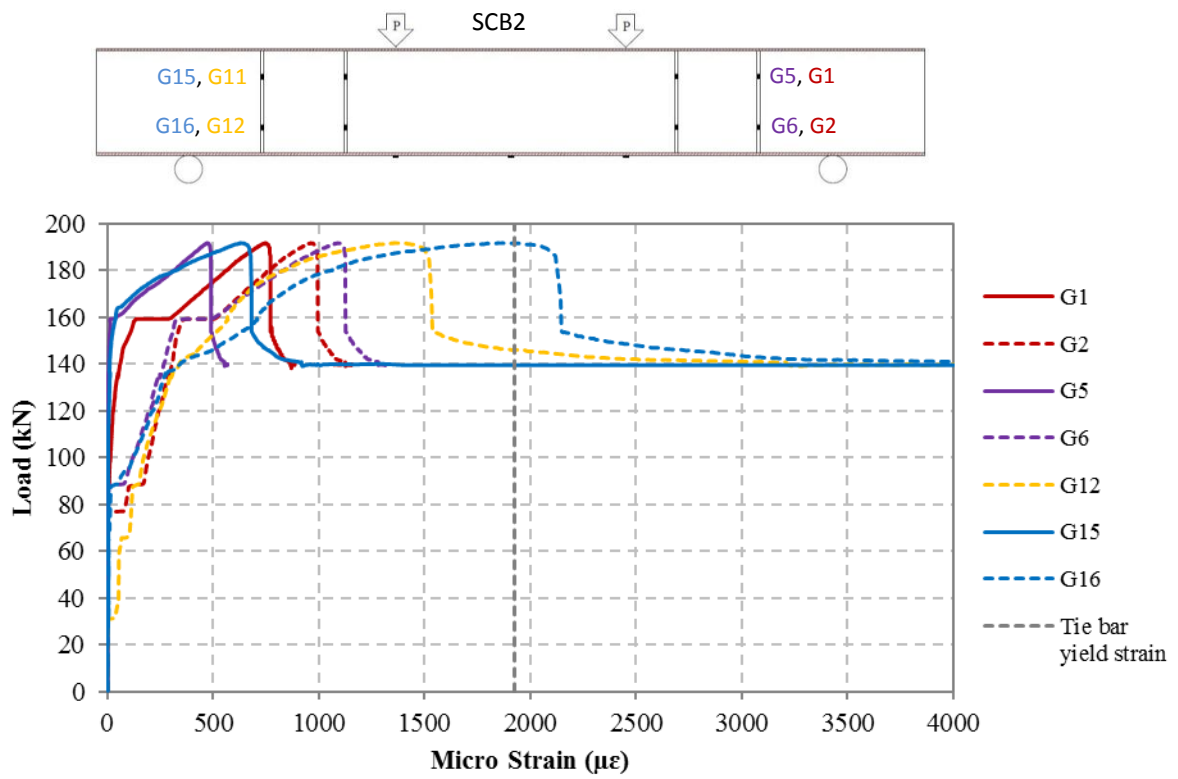
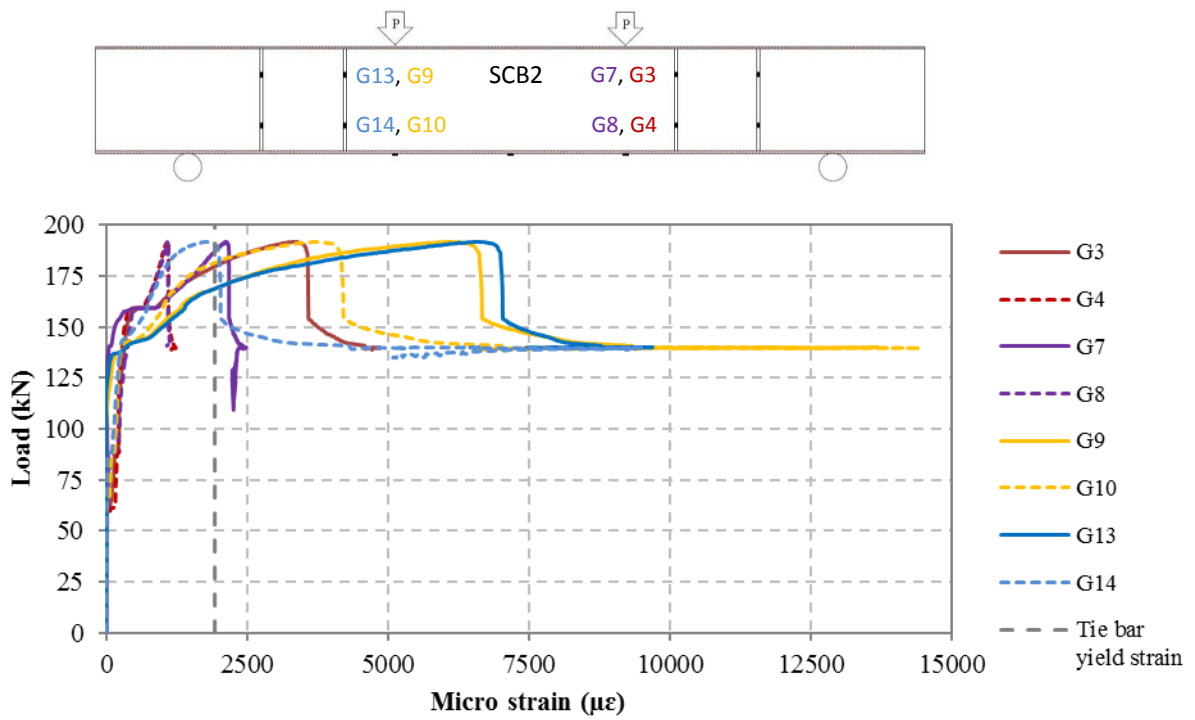


Figure 14: Measured strain for: (a) inner tie bars; (b) outer tie bars for SCB2

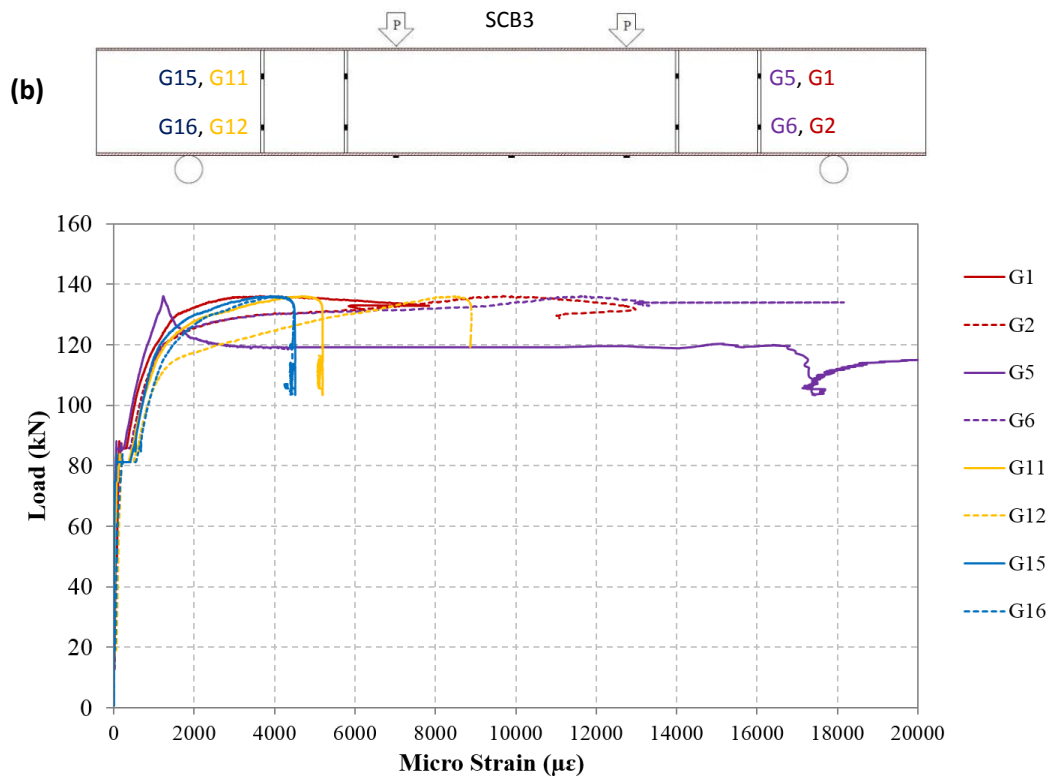
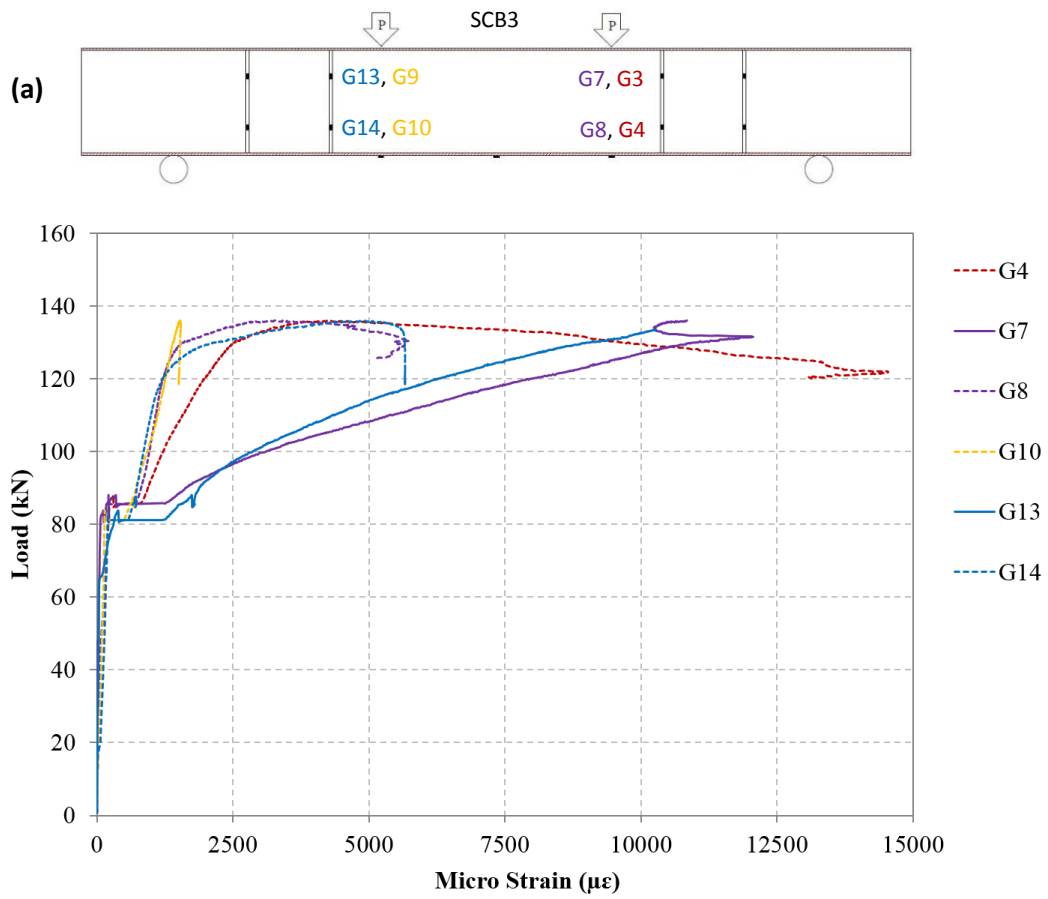


Figure 15: Measured strain for: (a) inner tie bars; (b) outer tie bars for SCB3

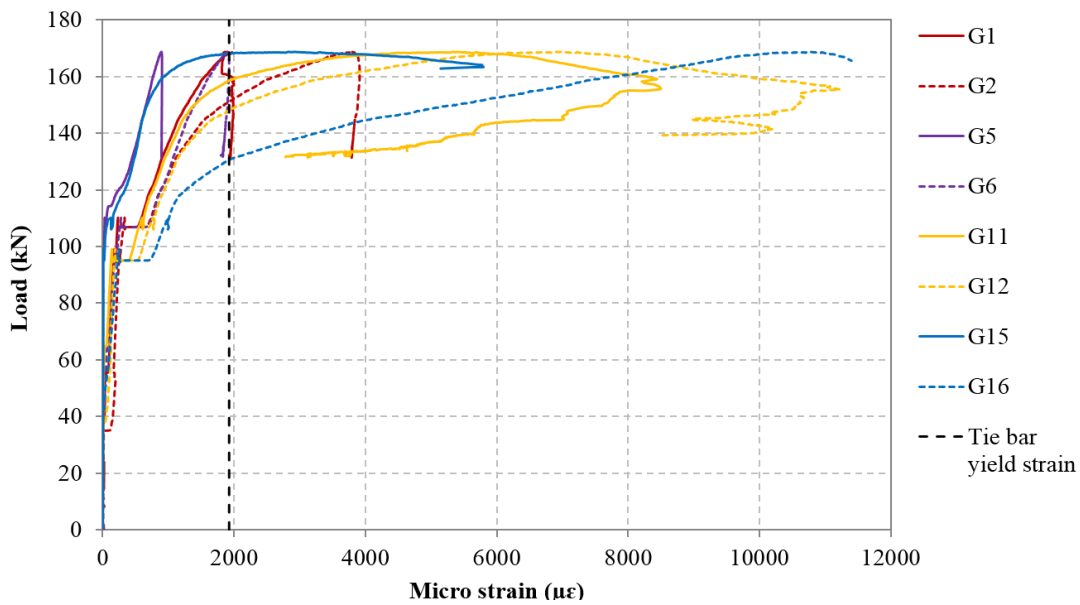
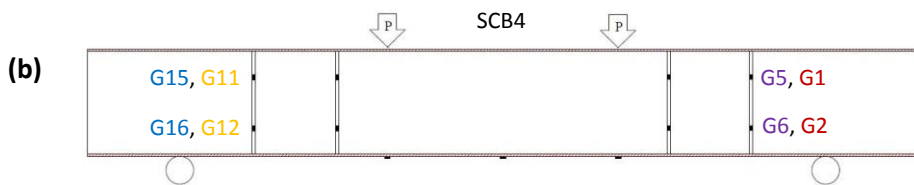
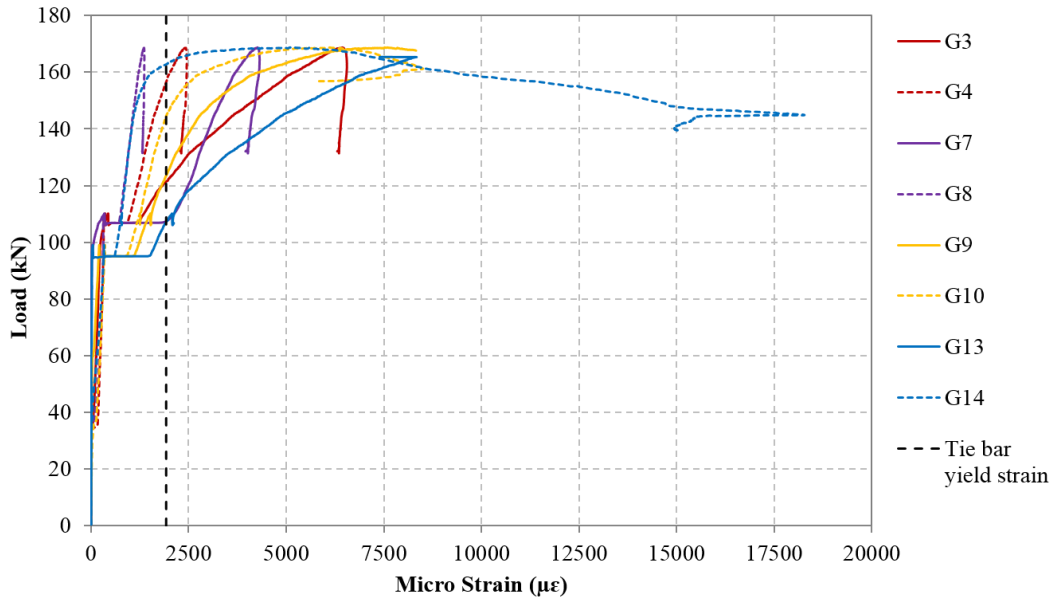
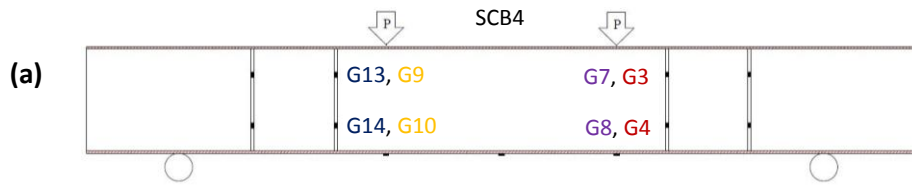


Figure 16: Strain measurements for: (a) inner tie bars; (b) outer tie bars for SCB4

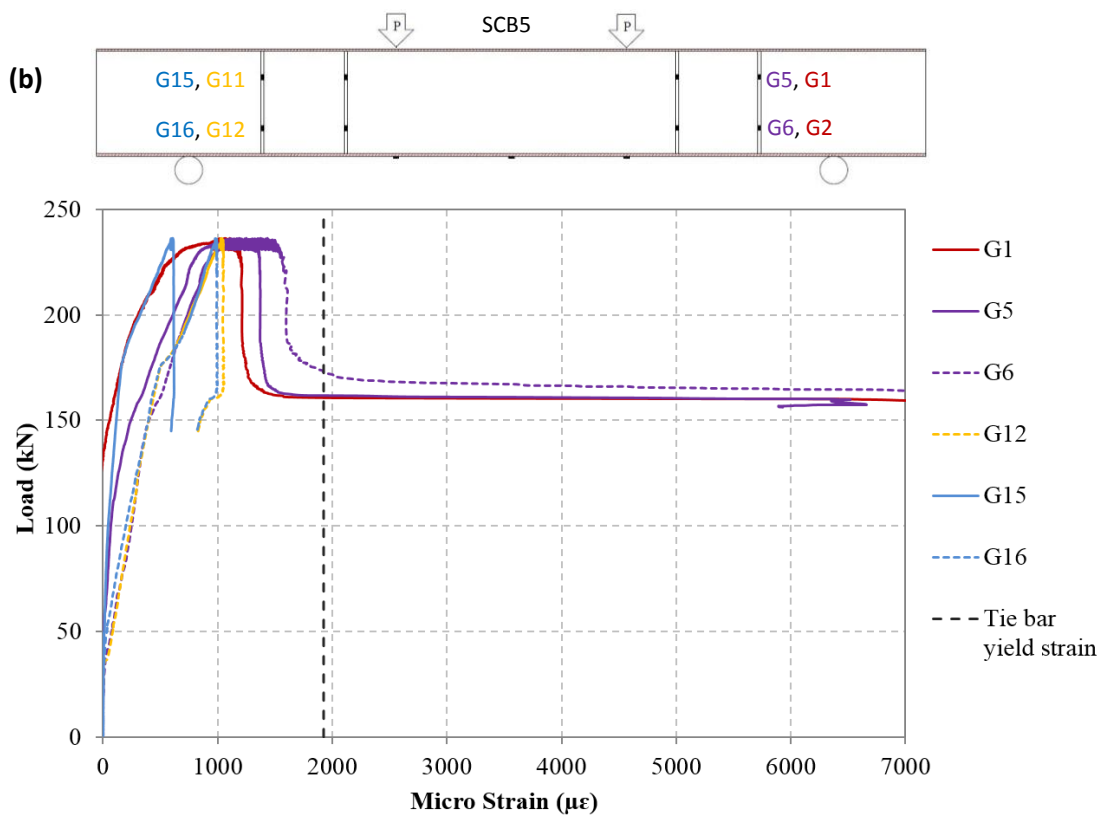
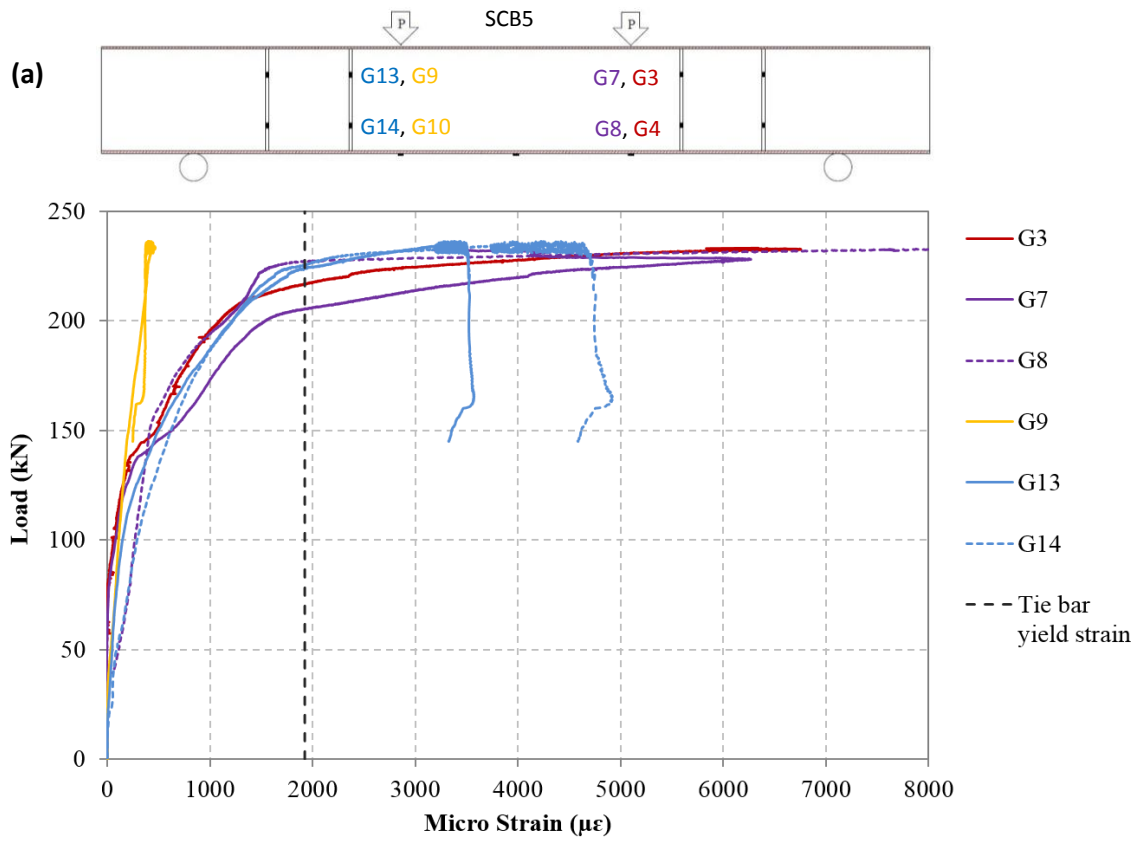


Figure 17: Measured strain for: (a) inner tie bars; (b) outer tie bars for SCB5

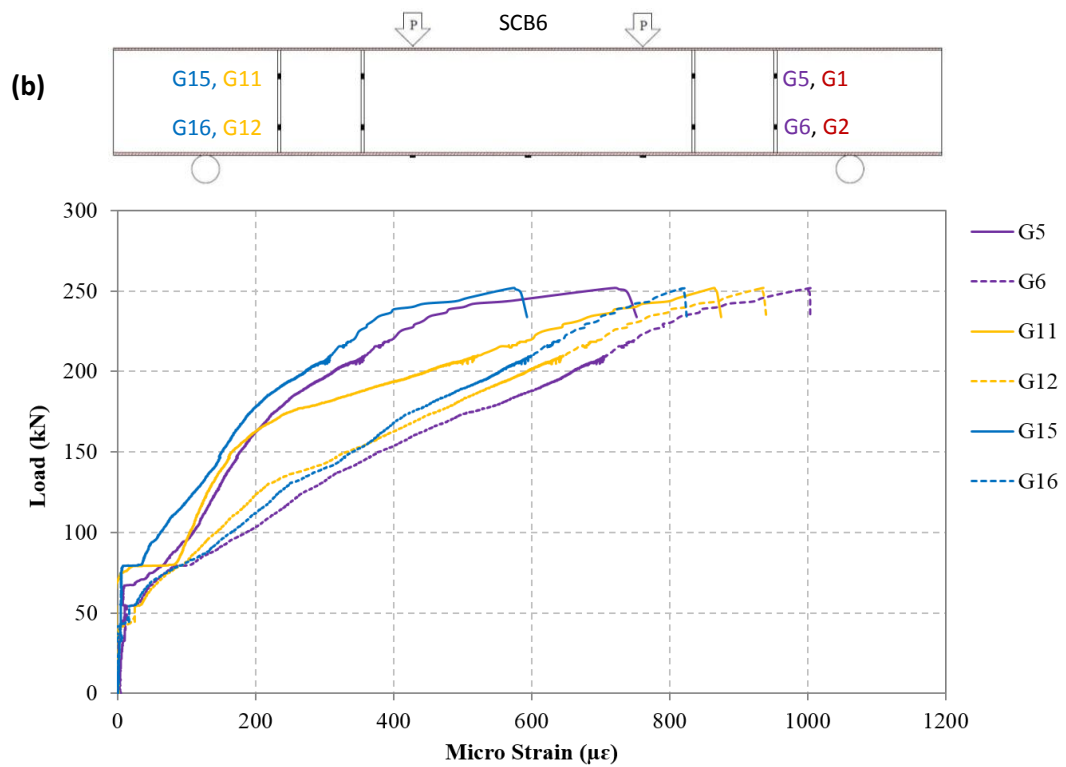
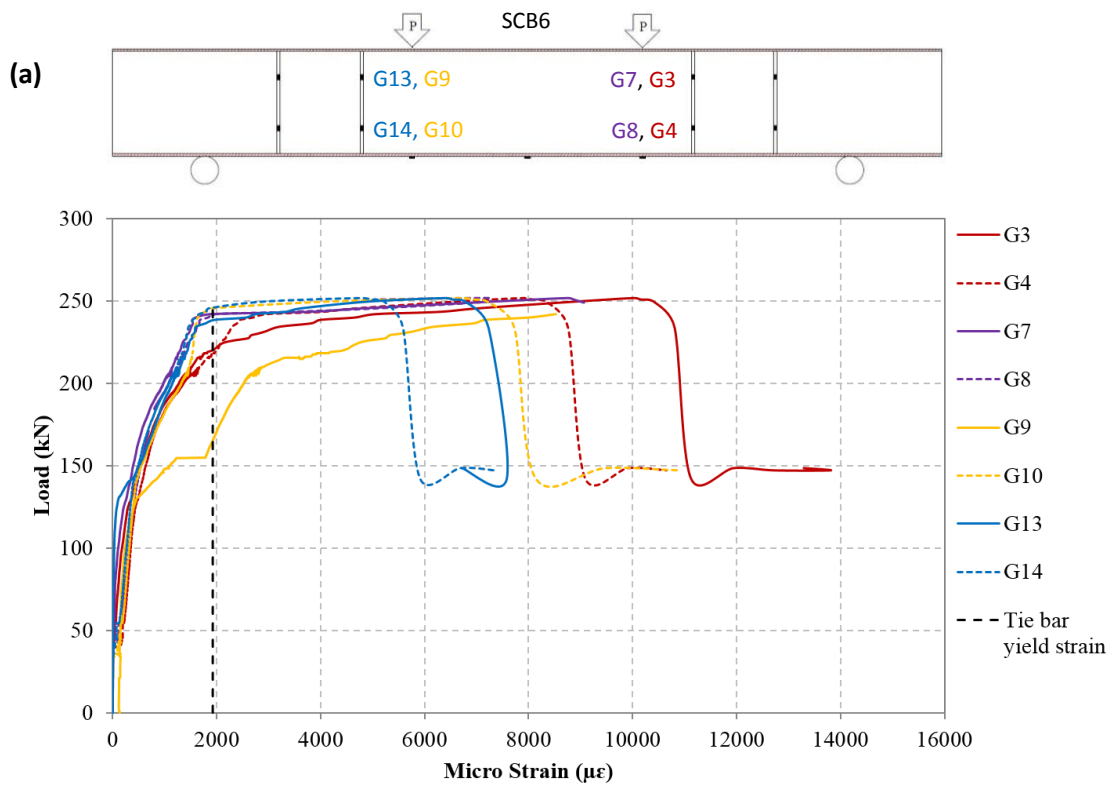
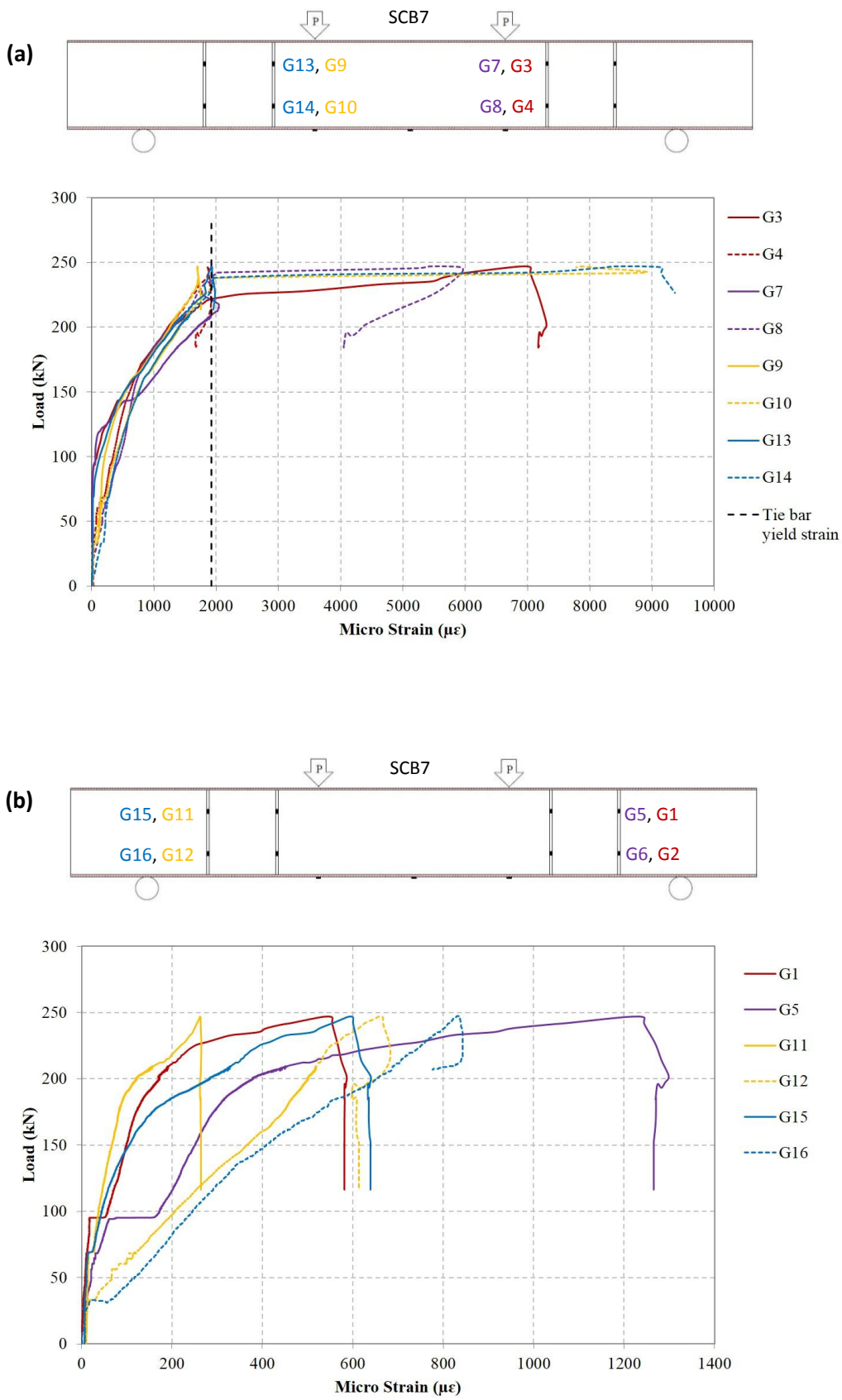


Figure 18: Measured strain for SCB6: (a) inner tie bars; (b) outer tie bars



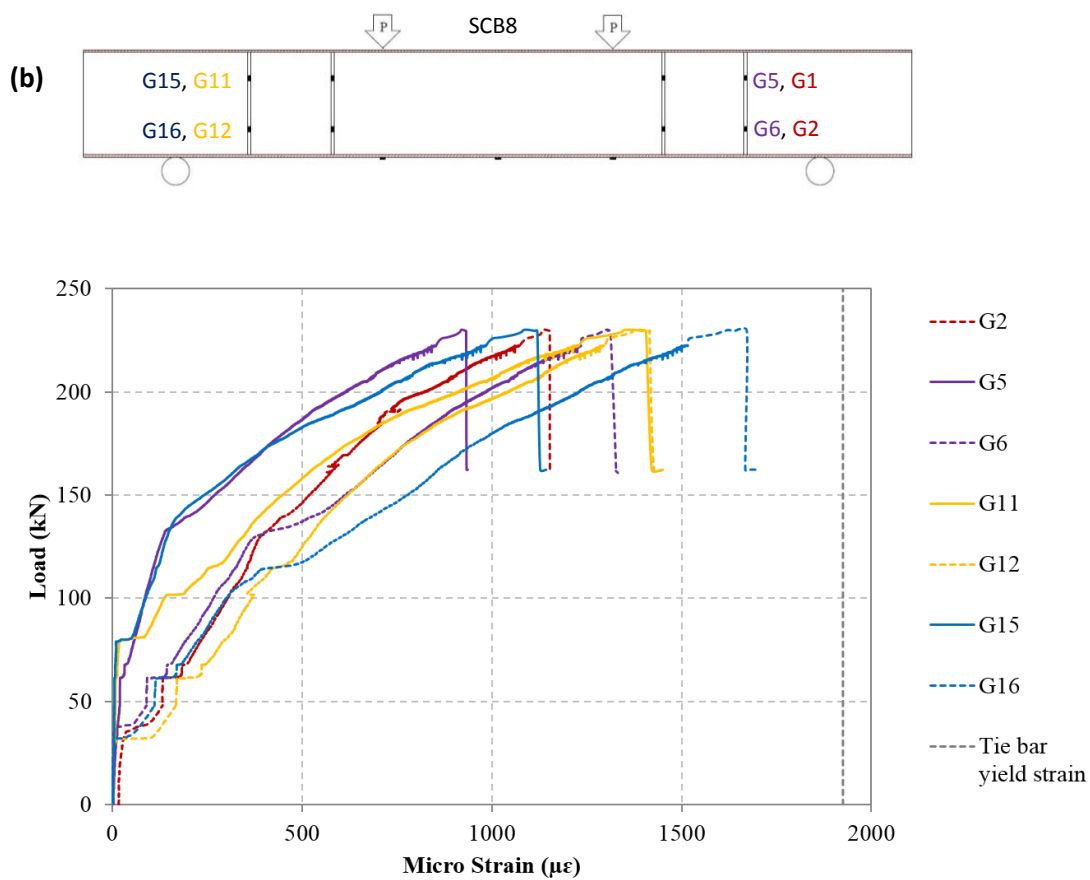
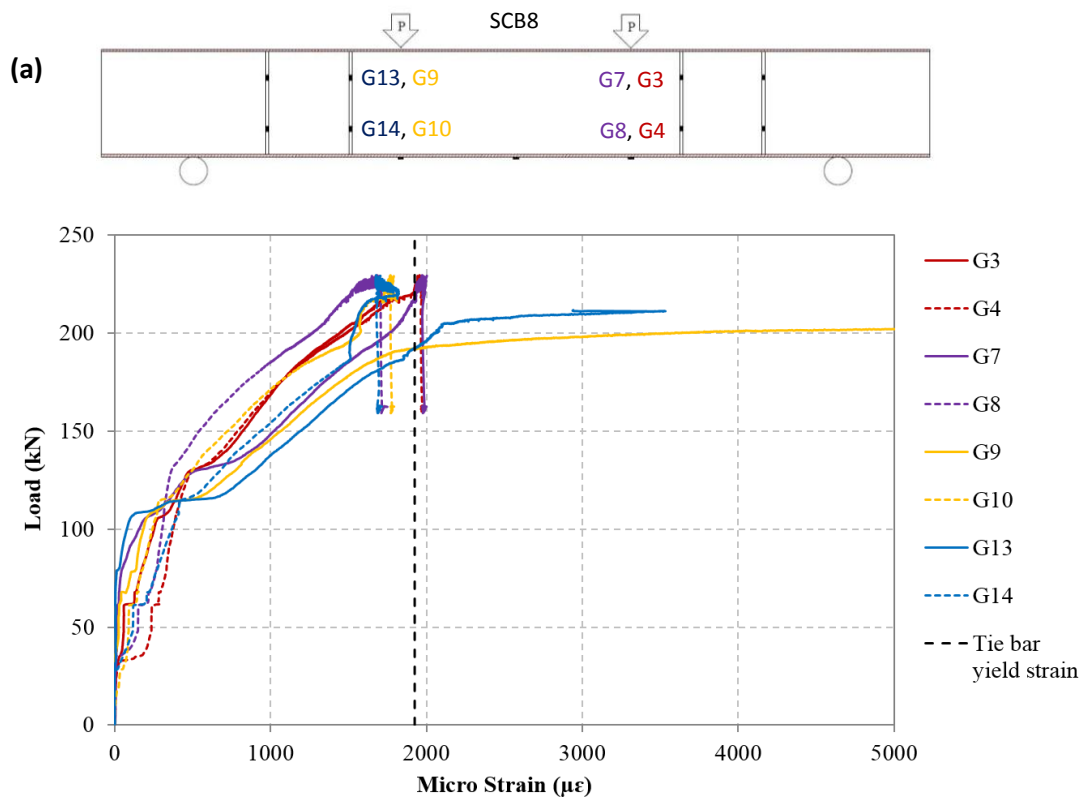
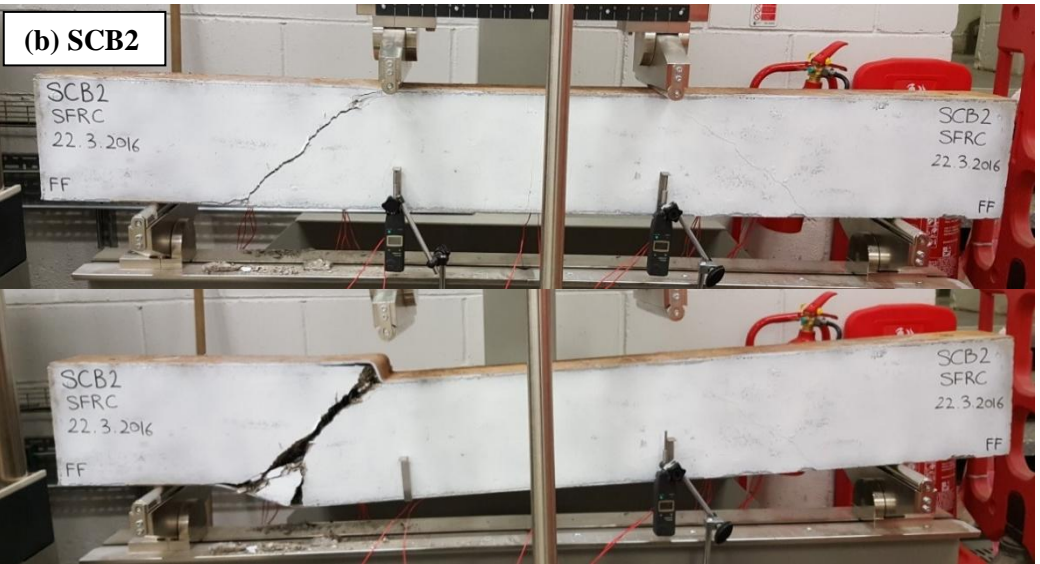
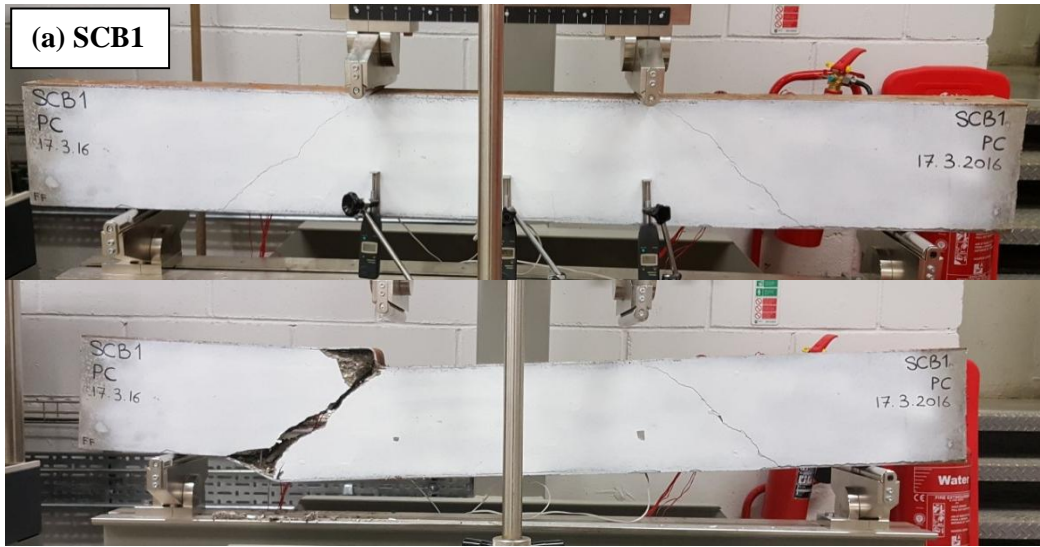


Figure 20: Measured strain in tie bars for: (a) outer bars; (b) inner bars for SCB8



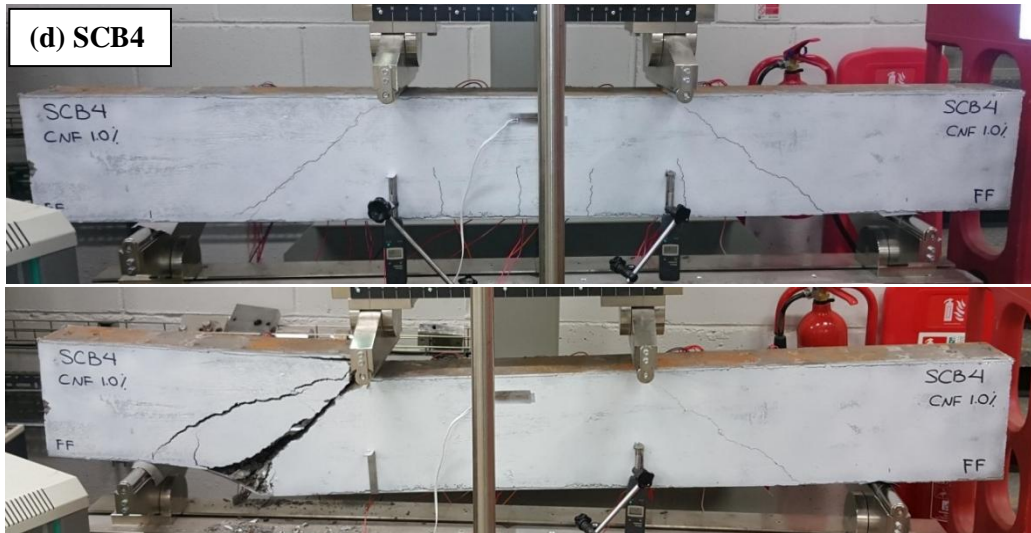


Figure 21: crack pattern of category 1 SC samples at ultimate load stage and at failure.



Figure 22: Steel plate local buckling of SCB1



Figure 23: Fractured tie bars in SCB1

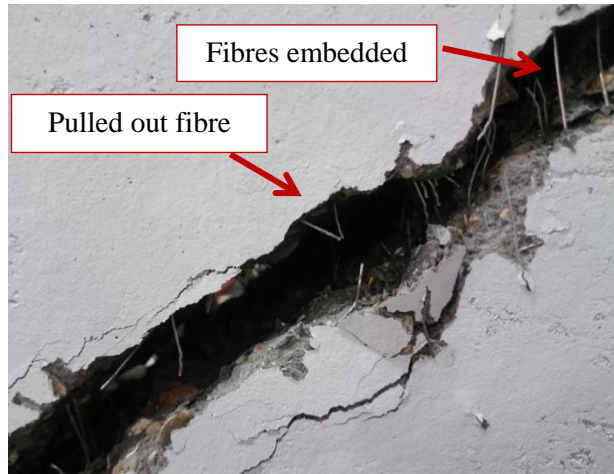


Figure 24: Close observation of shear crack for SCB8

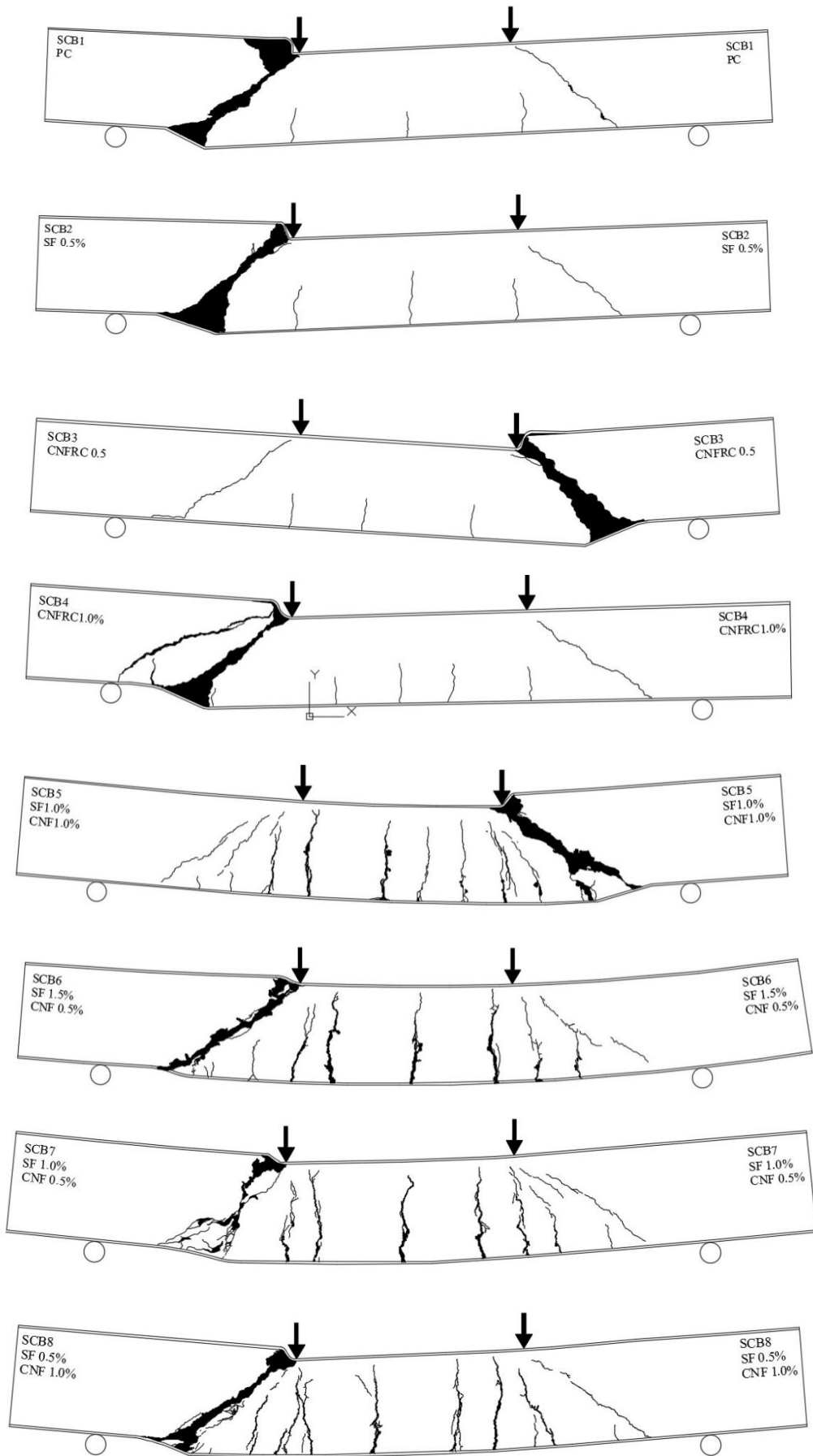


Figure 25: Crack map for all tested SC beams under four-point bending